[redacted]

Copy 230
RM E51F26

NACA RM E51F26

E 51 F26

TECH LIBRARY KAFB, NM
0143251

9899

RESEARCH MEMORANDUM

INVESTIGATION AT MACH NUMBER 1.91 OF SIDE AND BASE PRESSURE DISTRIBUTIONS OVER CONICAL BOATTAILS WITHOUT AND WITH JET FLOW ISSUING FROM BASE

By Edgar M. Cortright, Jr., and Albert H. Schroeder

Lewis Flight Propulsion Laboratory
Cleveland, Ohio

[redacted]

NATIONAL ADVISORY COMMITTEE
FOR AERONAUTICS

WASHINGTON
September 12, 1951

[redacted]

319.98/13

TECH LIBRARY KAFB, NM
0143251

NATIONAL ADVISORY COMMITTEE FOR AERONAUTICS

RESEARCH MEMORANDUM

INVESTIGATION AT MACH NUMBER 1.91 OF SIDE AND BASE PRESSURE DISTRIBUTIONS OVER CONICAL BOATTAILS WITHOUT AND WITH JET FLOW ISSUING FROM BASE

By Edgar M. Cortright, Jr., and Albert H. Schroeder

2228

SUMMARY

An experimental investigation has been conducted in a stream of Mach number 1.91 to determine the pressure distributions over the sides and bases of a systematic series of conical boattails. The effects on these pressure distributions of a jet issuing from the center of the base through a convergent nozzle were determined for a wide range of jet pressure ratios at body angles of attack up to 6°.

With no jet flow the method of characteristics overestimated the integrated boattail side pressure drag by approximately 20 percent; the experimental pressure distributions at zero angle of attack fell parallel to, but slightly less negative than the predicted values. Linearized theory gave somewhat poorer agreement. A semi-empirical theory is presented which enables the prediction of a base pressure coefficient referenced to conditions just upstream of the base for an arbitrarily boattailed body of revolution in a supersonic stream at zero angle of attack, provided the flow is unseparated upstream of the base. Good correlation was obtained between experimental and theoretical values of this coefficient. When the method of characteristics was utilized to predict the pressure upstream of the base, a fair estimate of the base pressure was obtained.

The effect of the jet on the external aerodynamics of the boattails was greatly dependent on the boattail geometry. When the boattail extended to a sharp edge at the nozzle exit (completely boattailed), the jet increased the pressures ahead of the base. As much as a 25-percent decrease in the boattail pressure drag resulted at a jet pressure ratio of 15. At low angles of attack, the pressure increases were asymmetrical on the boattail, which tended to shift the body center of pressure forward. When an annular base was present, the jet affected primarily the base pressure. The net effect of the jet for a cylindrical afterbody was approximately to double the annular base drag at a jet pressure ratio of 4; the drag was unaffected at a jet pressure ratio of 15. In the case

PERMANENT RECORD

of incompletely boattailed bodies with annular base, total boattail (side plus annular base) pressure drag increases of 25 to 40 percent were encountered at jet pressure ratios of approximately 3; drag decreases of 35 to 60 percent were obtained at a jet pressure ratio of 15.

Small amounts of jet air (base bleed) corresponding to values of jet pressure ratio of 1 or less decreased the base pressure drag. In the case of the cylindrical afterbody, increases of approximately 30 percent in base pressure coefficient were obtained at zero angle of attack. Increases of approximately 60 percent in base pressure coefficient were obtained for the boattailed bodies.

2228

INTRODUCTION

Supersonic missile and aircraft designs frequently utilize axially symmetric bodies or nacelles in which a propulsive jet discharges from the base. In many cases, the jet exit area is less than the maximum body cross-sectional area and some degree of boattailing is required. In some configurations the pressure drag of the boattail and annular base, if present, may far exceed the forebody pressure drag.

The choice of boattail geometry is complicated by the fact that no theoretical method for calculation of the external pressure distributions at supersonic velocities is currently available which considers the interference effects of an exiting jet. Despite this fact relatively little experimental work has been done to evaluate the phenomena. Preliminary studies of the jet effects on the external flow over the A-4 missile are presented in reference 1. A more recent aerodynamic investigation (reference 2) includes some effects of an annular jet exhausting from the base of a parabolic body of revolution at Mach number 1.92. Convergent-divergent nozzles with various exit velocities and pressure ratios were utilized and the body was fully boattailed to a sharp edge at the nozzle exit.

In the present investigation the pressure distributions over a limited but systematic series of conically boattailed bodies of revolution were obtained without and with a jet discharging from the center of the base. The jet exit nozzle was of the simple convergent type operating at various degrees of overpressure. The pressure distributions with no jet are compared with linearized theory and the method of characteristics. A semi-empirical theory is developed which enables the prediction of a base pressure coefficient referenced to conditions just upstream of the base for an arbitrarily boattailed body of revolution in a supersonic stream of zero angle of attack, provided the flow is unseparated upstream of the base. The effects of the jet on both the boattail side and annular base pressure distributions are experimentally determined. Integrated boattail pressure drag coefficients are presented and are compared from the standpoint of optimum boattail geometry.

2228

SYMBOLS

The following symbols are used in this report:

C_D drag coefficient, drag/$q_0 \frac{\pi D_M^2}{4}$

C_p pressure coefficient, $\frac{p-p_0}{q_0}$

$C'_{p,b}$ base pressure coefficient referenced to condition just upstream of base, $\frac{p_b-p_1}{q_1}$

$C_{p,j}$ increment of pressure coefficient due to jet air flow

$C_{p,\alpha}$ increment of pressure coefficient due to angle of attack

D_b base diameter of body, (in.)

D_m maximum body diameter, (in.)

D_n nozzle exit diameter, (in.)

M Mach number

M_j theoretical jet Mach number, $M_j = \left\{ \frac{2}{\gamma-1} \left[\left(\frac{P_j}{p_\alpha} \right)^{\frac{\gamma-1}{\gamma}} - 1 \right] \right\}^{1/2}$

M_l local Mach number measured in jet mixing region

P_j total pressure of jet air

P_p pressure measured by a pitot tube in jet wake

p static pressure

p_a ambient pressure for half-jet spreading tests

q dynamic pressure

U velocity of air at outer edge of boundary layer

u local velocity of air in boundary layer

V free-steam velocity

v_x axial perturbation velocity

x	axial distance from model tip, body diameters
y	normal distance from model surface
α	angle of attack, (deg)
δ	thickness of boundary layer at $u = 0.99\ U$
ϵ	angle between boattail surface and body axis, (deg)
θ	cylindrical coordinate measured in plane normal to body axis, $\theta = 0$ on windward side of model
ψ	free streamline angle at base measured with respect to the body axis

Subscripts:

b	base of model
0	free-stream station
1	station on model just upstream of base

APPARATUS AND PROCEDURE

Support System

In an investigation of jet effects on the external aerodynamics of bodies, one of the foremost experimental difficulties lies in introducing relatively large quantities of high pressure air into the model without influencing the external flow in the region of measurement. A hollow side strut support was utilized in reference 1. In order to avoid strut interference of the type resulting from such a support, reference 2 utilized a hollow sting and thus required an annular exit nozzle. In the present investigation an adaptation of a half-body support system was employed. A sketch of the model attached to the support is shown in figure 1 and a photograph of the model assembly in the tunnel is shown in figure 2. The model configurations were bodies of revolution composed of a single nose section with interchangeable bases that provided boattail variation. High pressure air was throttled and then ducted into the model through a hollow sting. In the model the air was turned (fig. 1) and passed through a straightening screen before discharge from a convergent nozzle. Support interference phenomena were limited by the presence of a splitter plate to those associated with plate boundary layer and small disturbances from the plate leading edge, which was swept back at an angle of 40°.

2228

Pressure disturbances reflecting from the tunnel walls did not intersect the jet wake at less than 12 exit nozzle diameters downstream of the base.

Nozzle Development

In order that the effects of the half jet on the external flow over the boattails be quantitatively meaningful, the half jet should closely approximate half of the axially symmetric jet which it is designed to simulate. Preliminary developmental tests were made to determine an internal geometry which would result in essentially constant Mach number distributions ahead of the nozzle inlet. The results of this development are shown in figure 3 where Mach number distributions are presented for jet pressure ratios P_j/p_a of approximately 2, 4, and 6. The final internal geometry which resulted in these profiles has been shown in figure 1. A jet wake in quiescent air downstream of a half nozzle was surveyed with the modified apparatus of reference 3. A comparison between the half-jet and full-jet boundaries defined as in reference 3 ($M_l/M_j = 0.11$) is shown in figure 4 for several downstream stations. Although the half jet was symmetrical, it was slightly smaller. Typical pitot pressure profiles in two planes of survey are presented in figure 5 for both the half jet and the full jet operating in quiescent air at a pressure ratio of approximately 4.6. The agreement in jet profile was quite good despite the fact that the half jet was slightly smaller in the mixing region. In general, these discrepancies between the half jet and the full jet are believed to have had no appreciable effect on the results of these experiments.

Models and Instrumentation

The assembled body of revolution had a length of 18 inches and a fineness ratio of 12. The first half of the body was contoured according to equation (14) of reference 1, while the remainder was cylindrical except as modified by the presence of conical boattails. Particular boattail geometries included in the investigation, along with the pressure instrumentation, are shown in figure 6. The parameters varied included boattail angle ϵ, 0°, 5.63°, 7.03°, and 9.33°; and base to body diameter ratio D_b/D_m of 0.506 (completely boattailed), 0.704 (incompletely boattailed), and 1.0 (cylindrical afterbody). The nozzle-exit to body diameter ratio was constant at 0.5. The nozzle profile was contoured for a constant Mach number gradient based on one-dimensional considerations.

Jet total pressures were normally determined at the nozzle entrance (fig. 1) by a pitot tube rake which was connected to a mercury manometer board. Low jet pressures and all static pressures were measured with a dibutylphthalate manometer board (referenced to vacuum), which was read

visually to ±0.02 inch. All static orifice diameters were 0.015 inch. Pitot tube rakes were utilized for boundary-layer surveys in the plane of the base at arbitrary angular stations θ.

Test Conditions and Procedure

2228

The experiments were conducted in the 18- by 18-inch (Mach number 1.91) supersonic wind tunnel at the NACA Lewis laboratory. Test-section total temperature and pressure were approximately 150° F and atmospheric, respectively. Ambient pressure in the region of the model was determined by a tunnel calibration which indicated no appreciable axial pressure gradients to exist. The Reynolds number in the test section was approximately 3.24×10^6 per foot. The dew point was maintained within the range from -10° to 3° F.

External pressure distributions were recorded at angles of attack $\alpha = 0°$, 3°, and 6° for values of jet pressure P_j/p_0 ranging from that corresponding to no jet flow to approximately 15. Angle of attack was varied in the plane of the splitter plate. Because only one quadrant of the base was instrumented, it was necessary to vary the angle of attack in both the positive and negative directions. For selected settings data were obtained with a loop of 0.005-inch-diameter wire approximately 0.5 inch from the tip of the model to induce early transition of the boundary layer.

DISCUSSION OF RESULTS

Boattail-Side-Pressure Distributions at Zero Angle of Attack

No jet. - The experimental pressure distributions on the sides of the six boattailed configurations at zero angle of attack are presented in figures 7 and 8. Pressure coefficient C_p is plotted as a function of axial distance from the model tip x in each of three angular planes $\theta = 15°$, 50°, and 90°. Mean pressure distribution curves are faired through the data. The flow over the conical boattails was characterized by the sudden expansion to a low pressure at the start of the boattails followed by recovery toward ambient pressure. Increasing the boattail angle increased both the initial expansion and the axial pressure gradient over the boattail, as expected. The small variation of pressure coefficient with θ is an indication that no large disturbances were caused by the splitter-plate leading edge or boundary layer.

A comparison of the mean experimental pressure distributions for all the boattail configurations with both linearized theory (reference 4) and the method of characteristics (reference 5) for the case of zero angle of attack and no jet flow is made in figure 9. Variation of pressure

2228

coefficient with axial distance from the boattail break (that is, the start of the boattail) is presented to permit pressure distributions of boattails of equal angle to be superimposed. In general, the experimental variations obtained with different boattails of equal angle agreed quite well. Mean distributions obtained with boundary-layer transition at the tip of the body (wire data) are included and show somewhat inconsistent but small departures from the natural transition case. Pressure distributions predicted by the method of characteristics fall parallel to but slightly more negative than the experimental values. Presence of the body boundary layer would be qualitatively expected to cause this deviation. Quantitatively, however, merely altering the conical boattail angle to some smaller effective value would not result in complete agreement of theory and experiment. The linearized theory of reference 4 was less satisfactory than the method of characteristics in predicting the pressure distributions, particularly for the larger boattail angles. In connection with the linearized theory, use of an approximate form of the pressure coefficient $C_p = -\frac{2v_x}{V}$ resulted in an improved prediction of the average pressure level on the boattail. With both linearized theory and the method of characteristics, the solutions were started at the beginning of the boattail by assuming uniform flow at this station.

Data for the cylindrical afterbody configuration are presented in figure 10, where they compare well with the mean of all the experimental data upstream of the boattails for the other model configurations. The pressure distribution predicted by linearized theory is also included for comparison. The mean of the experimental pressure coefficients deviates a maximum of 0.01 from the theory.

With jet. - The experimental pressure distributions on the sides of the three completely boattailed configurations at zero angle of attack are presented in figures 11 to 13 for jet pressure ratios ranging from values corresponding to no jet flow to approximately 15. The effect of the jet was generally similar to that observed in references 1 and 2 and was qualitatively independent of boattail angle. Increasing the jet pressure ratio from the no-flow value caused the pressure coefficient to increase upstream of the base. The pressure rise on the boattail increased with increasing jet pressure ratio and resulted in local regions of considerable thrust at large values of jet pressure ratio.

Since the jet effect of the external flow was confined to the rearmost portion of the bodies, the instrumentation was somewhat inadequate; a questionable extrapolation of the pressures was necessitated from the last orifice to the end of the body. Two steps were taken to check these extrapolations: (1) a static orifice was added at a distance 0.03-inch upstream of the base in the $\theta = 90^\circ$ plane of the 5.63° boattail; and (2) at the high jet pressure ratios, where the boundary-layer rake data indicated separated flow at the base, the rake pitot pressure in the

separated region close to the body surface was assumed equal to the static pressure. In figure 11(c), the unflagged data points at axial station $x = 12$ were obtained with the additional static pressure orifice. The previously extrapolated pressure distribution at a jet pressure ratio of 15 checks the additional orifice data very well. At lower jet pressure ratios the extrapolated curves appear to underestimate the jet effect. The double flagged symbols were obtained from the boundary-layer rake data with separated flow; these data check the static orifice quite well. In figures 12 and 13, additional data points obtained with the boundary-layer rake in the $\theta = 90^\circ$ plane are indicated. On these boattails the static pressures at the end of the body were indicated to be the same at jet pressure ratios of 8 and 15, possibly as a result of the rakes themselves influencing the local separation.

2228

In general, the check points were insufficient to determine a reliable extrapolation procedure for all the data; hence, no changes were made in the original extrapolations. They do indicate, however, possible inaccuracies in the curves as presented in that the reduction in boattail pressure drag due to the jet effect is slightly underestimated for jet pressure ratios below 15. This point will be discussed in a later section in which the integrated pressure drags are considered.

The flow mechanism whereby the jet interference takes place is illustrated by schlieren photographs and a qualitative sketch of the flow over the $\epsilon = 9.33$ fully boattailed configuration (fig. 14). As the jet pressure ratio is increased, the exiting jet expands and deflects the external flow with a resulting shock wave and pressure rise. This increased pressure propagates upstream through the subsonic portion of the boundary layer on the body; an increased rate of boundary layer growth and thus compression toward the rear of the body result with possibly a region of separated flow ahead of the base. Schlieren photographs of the three fully boattailed configurations operating at a jet pressure ratio of 15 are shown in figure 15 to indicate the similarity of flow fields. In figure 16 the 7.03° boattail is shown with artificially induced boundary-layer transition at the tip of the model. The thickened boundary layer was no longer distinct in this condition and the trailing shock wave with the jet in operation appeared to stand farther upstream than with the thinner boundary layer.

Inasmuch as the interference problem is largely one of shock boundary-layer interaction, the quantitative results of figures 11 to 13 would be expected to be sensitive to the boundary-layer thickness and profile at the base and hence to Reynolds number and surface condition of the body. The investigations with artificial boundary-layer transition to turbulence at the model tip were made to determine this sensitivity. In general, the data (figs. 11 and 13) indicated an appreciably increased

pressure rise at the base of the body due to the jet but no marked extension of the interference effect farther upstream as a result of thickening the boundary layer. As an apparent result of this sensitivity combined with probable slight variations of the body boundary layer during the course of the investigation, some difficulty with reproducibility of pressure distributions with jet was experienced. It can be concluded that the jet interference effect for completely boattailed bodies is dependent on the body Reynolds number and surface conditions.

2228

In the case of the incompletely boattailed configurations the annular base served largely to prevent interaction effects of the jet on the sides of the boattail. An exception was the 9.33° boattail, which showed a slight effect of the jet (an increase of 0.025 in C_p) at the downstream orifice in the $\theta = 90^\circ$ plane at a jet pressure ratio of 15. Schlieren photographs and a qualitative sketch which illustrate the absence of jet effect on the flow over the sides of these boattails are presented in figure 17 for the 7.03° boattail. No appreciable thickening of the boundary layer on the body is discernable even at the highest jet pressure ratio. The fact that a strong shock wave was formed by the meeting of the jet and external streams in the vicinity of the annular semi-dead air region at the base would indicate, however, that the jet might strongly affect the base pressure. This was found to be the case and will be discussed fully when the base pressure data are considered.

Boundary-Layer Measurements at Zero Angle of Attack

In order to supplement the static pressure distributions and schlieren photographs in depicting the flow over the boattails, limited boundary-layer surveys were made at the base of the boattails in radial planes of the static orifices. The data were obtained by means of survey rakes and, although they are not considered quantitatively precise, some important qualitative observations can be made.

In figure 18, the boundary-layer velocity profiles measured at $\theta = 90^\circ$ for the case of no jet flow are presented for all the model configurations tested. The corresponding values of boundary-layer thickness δ are included. The profiles were calculated by extrapolating the body static pressures from the last orifice to the plane of the base and then assuming the static pressure and total temperature constant through the boundary layer. The experimental values of δ correspond to the point in the boundary layer where the local velocity u equals 0.99 times the local free-stream velocity. As can be seen in figure 18(a) (incompletely boattailed bodies), the boundary-layer flow appeared to be turbulent. The von Karman one-seventh power profile for turbulent, incompressible, two-dimensional boundary layer is included for comparison. As the boattail angle became steeper and the pressure gradient

more adverse, the boundary-layer profile changed somewhat. The boundary-layer thickness varied between 0.08 and 0.09 inch except in the case of the boattail $\epsilon = 5.63$. Here inadvertant early transition to turbulence forward on the body (probably due to a leaking static orifice near the nose) resulted in a thickness of 0.20 inch. The main effect of this increased thickness was to produce an irregularity in the base pressure data that will be discussed subsequently. The boundary-layer profiles on the completely boattailed bodies (fig. 18(b)) were again apparently turbulent but were all distorted from the one-seventh power profile possibly as a result of the longer run in the presence of adverse pressure gradient or as a result of the increased ratio of boundary-layer thickness to base radius, or both. The boundary-layer thicknesses were nearly constant at 0.10 inch. The variations in boundary-layer profile that resulted from changing the boattail geometry probably did not greatly affect the base pressures. This fact simplified the analysis of the effect of boattail geometry on base pressure which will be considered subsequently.

2228

When boundary-layer transition was forced at the tip of the model by means of a 0.005-inch wire, the effect was to thicken the boundary layer greatly without significantly changing the profile, as shown in figure 18(a).

The boundary layer was not generally constant around the bodies as illustrated by figure 19 which presents boundary layer profiles at $\theta = 15^\circ$, 50°, and 90° for the 7.03° boattail. This was probably a result of the influence of the splitter plate, since some of the plate boundary layer would be expected to flow from the plate onto the lower pressure boattail. The boundary layer in the $\theta = 15^\circ$ plane was approximately 30-percent thicker than in the $\theta = 90^\circ$ plane and its profile was nearer that of the cylindrical afterbody.

When the bodies were boattailed to a sharp edge at the nozzle exit, the effect of the expanding jet on the boundary layer was pronounced (fig. 20). At a pressure ratio of 10, for example, the boundary layer was separated from the body with a greatly increased effective thickness. The thickening effect was greater for the steeper boattails.

Increments in Boattail Pressure Distributions

Due to Angle of Attack

The effects of angle of attack on the boattail pressure distributions are presented in terms of the increments in pressure coefficient due to angle of attack $C_{p,\alpha}$. These data were obtained by subtracting the pressure coefficient at any point at zero angle of attack from the value at the same point at angle of attack. Figure 21 presents $C_{p,\alpha}$ as a

function of circumferential station at angles of attack of 3° and 6° for all boattail angles investigated. These data are compared with variations obtained by use of linearized theory. (See, for example, reference 6.)

$$C_{p,\alpha} = 4\alpha \cos\theta \frac{dr}{dX} + \alpha^2 (1 - 4 \sin^2\theta) \qquad (1)$$

2228

where $\frac{dr}{dX} = -\epsilon$ and α is in radians. This expression, which applies for very slender bodies, is not expected to yield good agreement with experiment in the vicinity of a discontinuity in surface slope.

In figure 21(a) the variations of $C_{p,\alpha}$ are presented for the cylindrical afterbody configuration. Although the variation with circumferential station is generally as predicted, there is considerable scatter among the data for various axial stations. The data for the boattail configurations are presented in figures 21(b) to 21(d). In general, the increments in pressure coefficient due to angle of attack are negative on the windward surface and become positive on the leeward surface (where windward and leeward are taken with respect to the cross flow). At the farthest downstream station on the boattail the agreement between experiment and theory is in general superior to that at the other axial stations except, of course, for large values of θ where separation of the cross flow results in a pronounced departure of experiment from theory at all axial stations. Whether the increased discrepancy between experiment and theory near the start of the boattail resulted from the abrupt change in body slope or resulted from support system interference remains undetermined. The fact that boundary layer from the splitter plate flows onto the windward surface of the body at angle of attack and that, in addition, the splitter plate might influence the nature of the cross-flow separation on the leeward surface gives some reason to question the suitability of the present support technique for investigation of flow at angle of attack.

Increments in Boattail Pressure Distributions

Due to the Jet

The effects of the jet on the pressures acting over the completely boattailed configurations are shown in figure 22. The increment in pressure coefficient due to the jet $C_{p,j}$ is plotted as a function of circumferential station θ for each angle of attack including $\alpha = 0$ for reference. Data are presented for those axial stations experiencing an effect of the jet. The quantity $C_{p,j}$ was obtained by subtracting the pressure coefficient with no jet from the pressure coefficient at

the same point and angle of attack but with the jet in operation. At zero angle of attack the interference effect of the jet was nonuniform around the body. At an angle of attack of 3° the effect of the expanding jet was most pronounced in the region of thick boundary layer on the leeward side of the body and in the windward corner; the body center of pressure thus tended to shift forward. At $\theta = 50°$ where the boundary layer had thinned considerably, the jet interaction effect was negligible except for the 9.33° boattail. At an angle of attack of 6° the jet interaction was fairly uniform around the body for most pressure ratios.

2228

The data for the $\epsilon = 5.63°$ boattail at an angle of attack of 6° appear unusual inasmuch as little jet effect is indicated. Actually this indicates that the region affected by the pressure feedback has shifted downstream of the last orifice. With forced boundary-layer transition, a jet effect similar to the $\alpha = 3°$ condition was observed. Also when the pressure orifice was added just upstream of the base at $\theta = 90°$, values of $C_{p,j}$ of 0.14 were indicated at a jet pressure ratio of 15.

Boundary-Layer Measurements at Angle of Attack

In order to aid in visualizing the effect of the jet at angle of attack, figure 23 presents pitot pressure contours at the plane of the base for the boattail of $\epsilon = 7.03°$ and $D_b/D_m = 0.506$. Pitot contours at zero angle of attack are included for reference (figs. 23(a) and 23(b)) and indicate only a slightly nonuniform jet effect around the body. In figure 23(c) the thickening of the boundary layer on the leeward surface of the boattail at 6° angle of attack with no jet is evident. At a jet pressure ratio of 10 (fig. 23(d)) the boundary layer has thickened about the entire body although the degree of uniformity is difficult to determine from these data.

Base Pressure Measurements

Only the pressures acting over the sides of the various boattail configurations have thus far been considered. Of equal interest is the problem of base pressures. The base pressure data are most conveniently discussed in two parts: the first part is concerned with base pressures with no jet flow, and the second part considers the pressures acting on the annular bases with jet flow.

No jet. - Flow fields have been hypothesized which lead to the fairly successful prediction of base pressure characteristics for bodies of revolution with cylindrical afterbodies in a supersonic stream. (See references 7 to 9.) In addition, considerable experimental base pressure data have been collected for such bodies (references 7, 10,

and 11, for example). No theoretical treatment and few data are available in the literature, however, which consider the effect of an arbitrary boattail geometry on base pressure.

A semi-empirical theory is presented herein to predict a base pressure coefficient $C'_{p,b}$ referenced to conditions just upstream of the base for an arbitrarily boattailed body of revolution at zero angle of attack in a supersonic stream, provided the flow is unseparated ahead of the base. The essential assumption of the method is that the free streamline angle ψ (measured with respect to the body axis) at the base of an arbitrary body of revolution is a function only of the local stream Mach number ahead of the base M_1 and of the boundary-layer thickness and profile ahead of the base. (Approximately the same results can be obtained by assuming dependence of ψ on M_0 rather than M_1. This assumption yields the correct result that base pressure is independent of boattail angle in the limiting case of vanishingly short boattails and would seem reasonable for short boattails in general where the flow field influenced by the boattail is small.)

2228

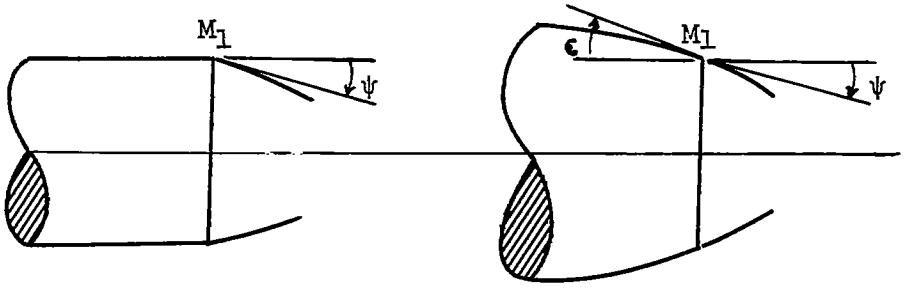

Cylindrical afterbody Arbitrary boattail

On the basis of the initial assumption, any body of revolution may be used to determine the variation of free streamline angle with Mach number ahead of the base. In the case of slender bodies with cylindrical afterbodies, the Mach number ahead of the base is approximately equal to the free-stream Mach number. Hence, by utilizing existing theoretical or experimental variations of base pressure with free-stream Mach number for such bodies, the desired variation of ψ with M_1 may be obtained simply with a knowledge of Prandtl-Meyer flow about a corner. This variation then applies by assumption to arbitrarily boattailed bodies or revolution provided the Reynolds numbers of the bodies are comparable. In practice, the effect of Reynolds number on base pressure is not great for values of Reynolds number sufficiently large to insure a fully developed turbulent boundary layer ahead of the base (reference 7).

For an arbitrary boattail the base pressure coefficient referenced to conditions just ahead of the base

$$C'_{p,b} = \frac{p_b - p_1}{q_1}$$

is a function only of the local Mach number just ahead of the base M_1 and the deflection angle $(\psi - \epsilon)$ of the flow in turning the base corner. The base pressure coefficient may be simply calculated from a knowledge of two-dimensional flow about a corner. (See reference 12 for example.)

2228

Base pressure coefficients referenced to free-stream conditions $C_{p,b}$ may be predicted for an arbitrary body by utilizing the method of characteristics to predict conditions at station 1 just ahead of the base. Then,

$$C_{p,b} = \frac{q_1}{q_0} C'_{p,b} + C_{p,1}$$

where

$$C_{p,1} = \frac{p_1 - p_0}{q_0}$$

The experimental base pressure coefficients $C_{p,b}$ and $C'_{p,b}$ determined from the pressure data of this report are presented in figure 24 as functions of boattail angle for all configurations tested. In addition the predicted variations are presented for comparison. Inasmuch as the Mach number just ahead of the base M_1 varied from 1.91 to 2.1 among the boattails, two predicted curves of $C'_{p,b}$ against ϵ covering this range of M_1 variation are presented. In calculating these curves the values of free streamline angle were determined from the data of references 7, 10, and 11. The agreement with the data presented herein is fairly good. Deviation of the experimental value of $C'_{p,b}$ for the $\epsilon = 5.63^\circ$ boattail with $D_b/D_m = 0.704$ may be qualitatively explained by the fact that early boundary-layer transition resulted in a large increase in boundary-layer thickness ahead of the base. (The effect of forced boundary-layer transition at the model tips was to increase the base pressure coefficients approximately 0.015.) A single value of $C'_{p,b}$ obtained from the tests of the parabolic body of revolution of reference 6 is included for comparison at $M = 1.9$.

In order to indicate the large predicted effect of Mach number on the variations of $C'_{p,b}$ with ϵ, curves for $M_1 = 1.3$ and 3.5 are also presented. The values of separation angle ψ for these curves were

estimated from unpublished data. At $M_1 = 1.3$, the values of $C'_{p,b}$ become appreciably positive at moderate boattail angles; the presence of relatively strong trailing shock waves at the base of the body is thus indicated.

An estimate of the base pressure coefficients referenced to stream conditions $C_{p,b}$ was obtained, as indicated in figure 24, with values of $C'_{p,b}$ calculated with the semi-empirical theory of this report and with the theoretical pressure coefficient just upstream of the base $C_{p,1}$ obtained from the characteristics solution. The base pressure coefficients estimated in this manner were somewhat low, which reflects primarily the deviation of theoretical from experimental pressures ahead of the base rather than an inability to predict the change in pressure due to separation at the base.

2228

The two-dimensional analogue to this method is of interest. Because the variation of M_1 is generally not great for a series of thin, blunt-trailing-edge airfoils, for example, the free streamline angle of the separated flow and hence base pressure in two-dimensional flow would be predicted to vary only slightly with airfoil profile.

The effect of angle of attack was to lower the base pressure, as has been previously observed by other experimenters (reference 6, for example). This is illustrated in figure 25, which presents the increment in base pressure due to angle of attack $(C_{p,b})_\alpha$ as a function of angle of attack for all configurations tested. Attempts to extend the previous semi-empirical theory to predict the effect of angle of attack on base pressure were unsuccessful.

The base pressures with no jet flow were determined with the base closed, inasmuch as slightly higher values were obtained with the base open. This was possibly a result of a known slight air leakage to the base region. With regard to air leakage into the base region it should be noted that the plate boundary layer provided a possible extraneous source of air influx through the low-energy portion of the boundary layer. The expected result would be values of base pressure slightly higher than for a complete body as was observed for the case of the cylindrical afterbody.

With jet. - The effect of jet flow on the pressures acting on an annular base region was determined in the case of the model with a cylindrical afterbody and the incompletely boattailed models of $D_b/D_m = 0.704$. These data are presented in figure 26 where base pressure coefficient is plotted as a function of jet pressure ratio. Base pressure coefficients are shown for various values of angular station θ on the base. In the case of the cylindrical afterbody, little variation of base pressure coefficient with radial distance on the base was observed; hence, the readings for the three orifices in each plane θ

were averaged. The pressure coefficients corresponding to the lowest recorded values of jet pressure ratio represent the values for no jet flow.

The jet effects were very great. When a small amount of air was permitted to flow into the base region, the base pressure coefficient increased approximately 30 percent, 0.04, for the cylindrical afterbody at zero angle of attack and approximately 60 percent, from 0.05 at zero angle of attack to 0.07 at a 6° angle of attack, in the case of the boattailed bodies. This increase in base pressure with small amounts of air flow to the base indicates the effectiveness of "base bleed" in reducing pressure drag, a technique first demonstrated to be effective in reference 13. As the jet pressure ratio increased beyond a value of approximately 1, the base pressure began to decrease rapidly until, at pressure ratios of approximately 4 and 3 for the cylindrical afterbody and the boattailed bodies, respectively, the base pressures reached minimum values which were considerably lower than the initial values. Further increases in jet pressure ratio increased the base pressure. In the case of the cylindrical afterbody with a jet pressure ratio of 15, the annular base pressure coefficient returned to approximately the original value. In the case of the boattailed bodies the base pressure coefficient at a jet pressure ratio of 15 increased to a positive value. The boattailed bodies at angle of attack indicated an appreciable variation of pressure coefficient around the annular base at the higher jet pressure ratios.

The effect of the jet at pressure ratios greater than those corresponding to the base bleed range may be explained in at least two ways. As the jet pressure ratio is increased, the jet velocity increases and entrains air from the semi-dead air annulus. This entrainment tends to lower the pressure on the annular base by an amount which increases with jet pressure ratio. As the jet pressure ratio increases, however, the jet expands; the shock wave located at the point of interaction of the jet and the free stream increases in intensity and causes a pressure feedback through the subsonic mixing region between the two streams with a resulting base pressure increase. A second qualitative explanation is that the jet displacement may act in a manner analogous to a center-sting support. Increasing the sting diameter causes the base pressure to approach the lower two-dimensional value (reference 7). The increasing jet displacement with increasing jet pressure ratio could thus qualitatively lower the base pressure, and the strong interaction shock would again cause a reversal of trend at the high pressure ratios.

Either of the preceding explanations would indicate that the ratio of nozzle exit diameter to base diameter might be expected to affect the variation of base pressure coefficient with jet pressure ratio in the range where base bleed effects do not predominate. Superposition of the faired curves of figure 26 indicates this to be true (fig. 27). For jet

2228

pressure ratios greater than 2, the faired curves were nearly identical at the three angles of attack for the cylindrical afterbody of nozzle to base diameter ratio $D_n/D_b = 0.50$. In the same pressure ratio range the faired curves for all the boattail configurations, $D_n/D_b = 0.71$, at all angles of attack were nearly the same, although some difference was noted at the highest pressure ratio. The wide separation of the two general variations indicated that the effect of D_n/D_b was large. With values of D_n/D_b approaching 1 the jet would, of course, begin to effect the side pressures also.

As a qualitative check on the effect of body Reynolds number on the variation of base pressure coefficient with jet pressure ratio, data were obtained with artificial transition at the nose of the body which resulted in a thicker boundary layer at the base. These data are presented in figure 26(a) for zero angle of attack. The thickening of the boundary layer serves only to displace the variation slightly in the positive direction.

Typical schlieren photographs of the flow in the base region of annular base bodies are shown in figures 15 and 28. Figure 28 illustrates the cylindrical afterbody configuration for the complete range of jet pressure ratios. The strong interaction of the jet and external flow is clearly evident.

Total Afterbody Drag

In order to examine the total drags of conical boattails the pressure data were integrated so as to yield pressure drag coefficients for all configurations tested at zero angle of attack. The results will be considered with no jet effect and with jet effect. The total boattail (afterbody) drag is broken down into side pressure drag, base pressure drag, and friction drag. With the jet discharging from the base, the base pressure drag is considered to be the drag of the annular bases.

No jet. - The variations of the components of boattail drag with boattail angle are presented in figures 29 and 30 for the bodies of base to body diameter ratios of 0.506 and 0.704, respectively. The side pressure drag decreases with boattail angle, as expected, reaching a minimum of zero at $\epsilon = 0$. The method of characteristics overestimated the side pressure drag by about 18 to 20 percent. Linearized theory in the form of reference 4 still further overestimated the pressure drag, although approximation of C_p by $-\frac{2v_x}{V}$ resulted in improved agreement with the method of characteristics for the particular boattail geometries considered.

Base pressure drag was observed to increase with decreasing boattail angle for the subject base to body diameter ratios. This variation is in accordance with the method of this report, although the method overestimated the base drag as a result of the deviation of theoretical and experimental pressures ahead of the base. The data point for $\epsilon = 5.63^\circ$, $D_b/D_m = 0.704$ is the point previously indicated as inconsistent as a result of inadvertent early transition of the boundary layer on the body.

The experimental value of base pressure drag coefficient at a boattail angle of zero was estimated by assuming that the base pressure obtained with the cylindrical afterbody would be the limiting pressure. Actually this indication would not be true since $\epsilon = 0$ corresponds to an indefinitely long boattail with an indefinitely thick boundary layer, which would indicate that the base pressure might approach ambient pressure (that is, $C_D = 0$). The actual variation might be expected to deviate sharply from the high pressure drag coefficient toward zero at small boattail angles.

Although the total boattail pressure drag decreased with decreasing boattail angle, the optimum angle for a given base to body diameter ratio must be determined by estimating the skin friction drag. If the boattail is assumed to be an appendage on the rear of a fixed forebody, the total body friction drag increases with decreasing boattail angle in the indicated manner for a local friction coefficient of 0.003. The result is that optimum boattail angles of approximately $\epsilon = 5.0^\circ$ and $\epsilon = 4.5^\circ$ are indicated for the configurations of base to body diameter ratio of 0.506 and 0.704, respectively. The boattail with the smallest base still yields the smallest minimum drag coefficient, but the difference is diminished by inclusion of friction drag. A smaller average friction drag coefficient would result in smaller optimum boattail angles. If geometric restrictions are placed on boattail or total body lengths, these allowances for friction drag must be modified. Hence, the actual optimum boattail angle may vary from those indicated, depending on the particular application.

Data points indicating base and total pressure drag with the optimum amount of "base bleed" for the incompletely boattailed bodies are also included in figure 30 to show the reductions in total pressure drag obtainable.

With jet. - The effect of an exiting jet on the boattail pressure drags is illustrated in figures 31 and 32. When there is a jet and no annular base, the total pressure drag coefficient is merely the side pressure drag (fig. 31). The percentage reduction in this drag coefficient from the no jet condition is roughly independent of boattail angle for a given jet pressure ratio, reaching a value of approximately 25 percent at $P_j/P_0 = 15$. For the low jet pressure ratios, the jet effect may be

2228

underestimated, as was already discussed when the pressure distributions with jet were considered (fig. 11). In the case of the 5.63° boattail, for example, the decrease in drag due to the jet at a pressure ratio of 6 may be nearly double that indicated. From a quantitative viewpoint, however, the possible error in over-all drag coefficient remains small and does not greatly lessen the value of figure 31. The drag decrements due to the jet effect considered only the $\theta = 50°$ and 90° data of figure 22.

2228

Presence of an annular base insulated the side of the boattail from jet effects, but the base drag was strongly influenced as shown in figure 32. The jet effects were nearly independent of boattail angle except at a jet pressure ratio of 15. The maximum drag condition, which occurred at a jet pressure ratio of 3, indicated a 100-percent increase in annular base pressure drag and a 25- to 40-percent increase in total boattail drag (side plus annular base) from the no jet condition. The minimum drag condition at a pressure ratio of 15 constituted an annular base pressure drag reduction of 100 to 190 percent and a total boattail pressure drag reduction of 45 to 60 percent.

In figure 33 boattail pressure drag coefficients are plotted as functions of boattail fineness ratio for all the configurations at three different pressure ratios. For each curve the data points at the largest fineness ratio were obtained from the bodies boattailed to a sharp edge at the nozzle exit ($D_b/D_m = 0.506$). The data points for zero-length boattail correspond to the cylindrical afterbody data and the intermediate points correspond to the boattails with annular bases. For the case of no jet flow with a full base (projectile condition, fig. 33(a)), the data indicate the desirability of complete boattailing, as would, of course, be expected from the boattail pressure distributions. With jet flow and when only the annular portion of the bases is considered (fig. 33(b)), the data indicate the desirability of boattailing to a sharp edge except at the high jet pressure ratios where the effect of the jet on the annular base is sufficiently favorable to make these configurations slightly superior. These curves may also be used to predict optimum geometries for a fixed boattail fineness ratio if such a restriction is present. In actual application, appropriate friction drag estimates must be considered.

SUMMARY OF RESULTS

The pressure distributions over conical boattails without and with jet flow issuing from the base were determined in a wind-tunnel investigation at a Mach number of 1.91. The jet nozzle was of the simple convergent type with the ratio of nozzle exit to body diameter equal to 0.50. The following results were obtained:

No Jet

1. The experimental pressure distributions over the sides of the boattails fell parallel to but above the potential flow distributions predicted by the method of characteristics. The approximate result was a 20-percent overprediction of side pressure drag by the theory. Linearized potential flow theory gave a somewhat poorer correlation than the method of characteristics.

2. A semi-empirical theory was evolved to predict a base pressure coefficient referenced to conditions just upstream of the base for an arbitrarily boattailed body of revolution in a supersonic stream at zero angle of attack provided the flow is unseparated upstream of the base. Good correlation was obtained between the experimental and theoretical values of this coefficient.

3. Determination of optimum boattail configurations depended largely on the assumption of skin friction drag, since pressure drag decreases monotonically with boattail angle. When the boattail was considered as an appendage on a fixed body and the average friction coefficient was assumed 0.003, the optimum angles were approximately 5.0° and 4.5° for the base to body diameter ratios of 0.506 and 0.704, respectively.

With Jet

1. The interaction effect of the jet on the body aerodynamics was largely a function of the body geometry. (a) For bodies completely boattailed to a sharp edge at the nozzle exit, the expanding jet increased the pressures upstream of the base and resulted in as much as a 25-percent decrease in boattail side pressure drag at a jet pressure ratio of 15. At low angles of attack the pressure increases were asymmetrical; the body center of pressure thus tended to shift foreward. These effects were sensitive to body boundary layer. (b) When an annular base was present, the jet affected primarily the base pressures. For the cylindrical body the annular base drag was doubled compared to the no-jet condition at a jet pressure ratio of 4 but was not affected at a jet pressure ratio of 15. For the incompletely boattailed bodies, afterbody (side plus annular base) pressure drag increases of 25 to 40 percent were encountered at jet pressure ratios of approximately 3 while drag decreases of from 45 to 60 percent were obtained at a jet pressure ratio of 15. (c) Jet effects were sufficiently great at the high jet pressure ratios to influence the determination of optimum boattail configurations.

2228

2. Small amounts of air flow into the base region ("base bleed") corresponding to jet pressure ratios of 1 or less resulted in base drag reductions of 30 percent for the cylindrical afterbody and 60 percent for the boattailed bodies at zero angle of attack.

2228

Lewis Flight Propulsion Laboratory,
National Advisory Committee for Aeronautics,
Cleveland, Ohio, May 21, 1951.

REFERENCES

1. Erdmann: Widerstandsbeiwerte für das A4V1P mit Berücksichtigung des Strahl - und Reibungseinflusses für Unter- und Uberschallgeschwindigkeiten-Untersuchung der Strahlexpansion. Peenemunde Heeresversuchsstelle Aerodynamisches Institut, Archiv Nr. 66/105, Mars 24, 1943.

2. Love, Eugene S.: Aerodynamic Investigation of a Parabolic Body of Revolution at Mach Number of 1.92 and Some Effects of an Annular Jet Exhausting from the Base. NACA RM L9K09, 1950.

3. Rousso, Morris D., and Kochendorfer, Fred D.: Experimental Investigation of Spreading Characteristics of Choked Jets Expanding into Quiescent Air. NACA RM E50E03a, 1950.

4. Brown, Clinton E., and Parker, Hermon M.: A Method for the Calculation of External Lift, Moment, and Pressure Drag of Slender Open-Nose Bodies of Revolution at Supersonic Speeds. NACA ACR L5L29, 1946.

5. Ferri, Antonio.: Application of the Method of Characteristics to Supersonic Rotational Flow. NACA Rep. 841, 1946.

6. Luidens, Roger W., and Simon, Paul C.: Aerodynamic Characteristics of NACA RM-10 Missile in 8- by 6-Foot Supersonic Wind Tunnel at Mach Numbers from 1.49 to 1.98. I - Presentation and Analysis of Pressure Measurements (Stabilizing Fins Removed). NACA RM E50D10, 1950.

7. Chapman, Dean R.: An Analysis of Base Pressure at Supersonic Velocities and Comparison with Experiment. NACA TN 2137, 1950.

8. Gabeaud: Base Pressures at Supersonic Velocities. Jour. Aero. Sci., vol. 16, no. 10, Oct. 1949, p. 638.

9. Cope, W. F.: The Effect of Reynolds Number on the Base Pressure of Projectiles. Eng. Div. 63/44, British Nat. Phys. Lab., Jan. 1945.

10. Kurzweg, H. H.: New Experimental Investigations on Base Pressure in the NOL Supersonic Wind Tunnels at Mach Numbers 1.2 to 4.24. NOL Memo. 10113, Naval Ord. Lab., Jan. 23, 1950.

11. Charters, A. C., and Turetsky, R. A.: Determination of Base Pressure from Free-Flight Data. Rep. No. 653, Ballistic Res. Lab., Aberdeen Proving Ground, March 30, 1948.

12. The Staff of the Ames 1- by 3-Foot Supersonic Wind-Tunnel Section: Notes and Tables for Use in the Analysis of Supersonic Flow. NACA TN 1428, 1947.

13. Cortright, Edgar M., Jr., and Schroeder, Albert H.: Preliminary Investigation of Effectiveness of Base Bleed in Reducing Drag of Blunt-Base Bodies in Supersonic Stream. NACA RM E51A26, 1951.

2228

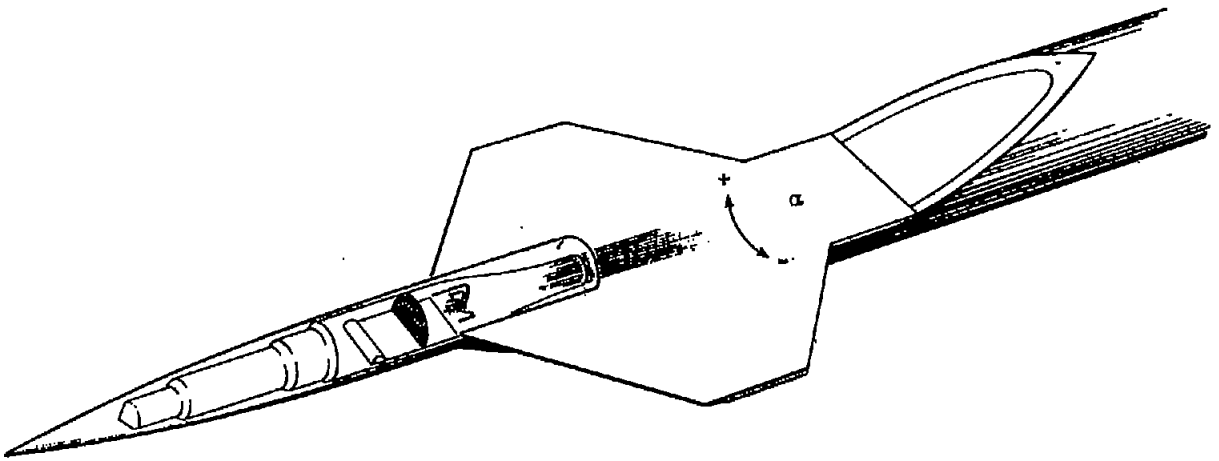

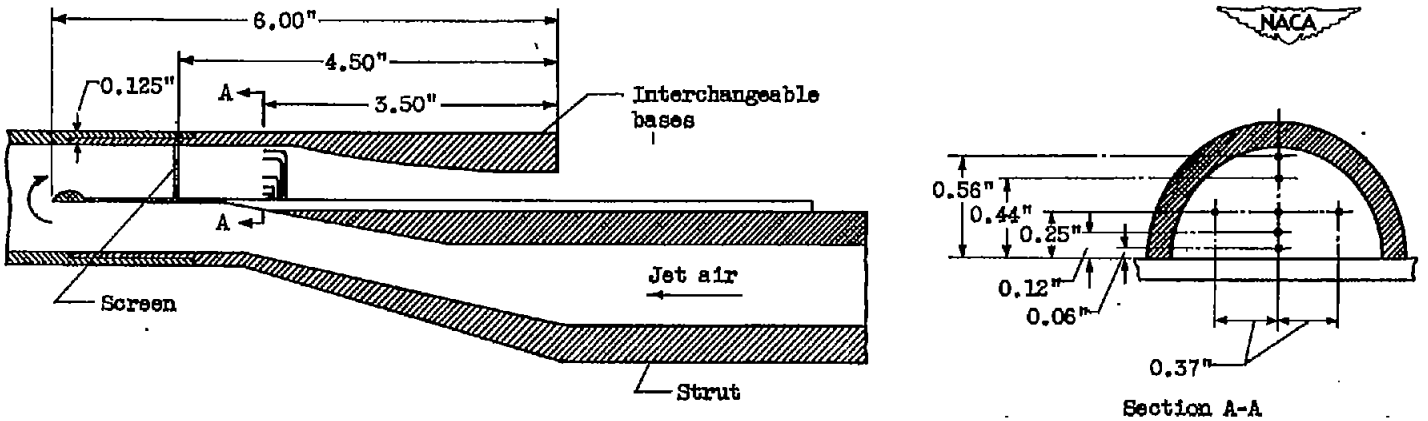

Figure 1. - Sketch of boattail model and support including cutaway section showing jet air flow in model and jet air pitot pressure rake.

Figure 2. - Photograph of model in 18- by 18-inch tunnel.

8222

2228

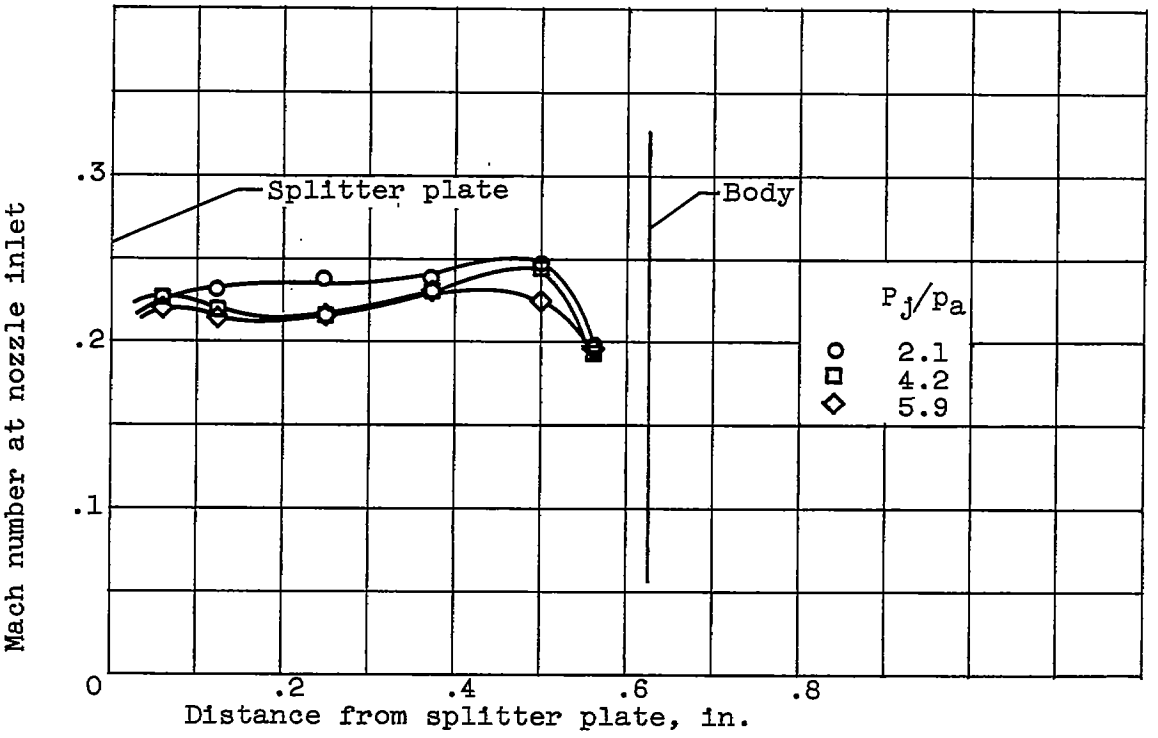

Figure 3. - Mach number profiles at center of nozzle inlet and normal to splitter plate.

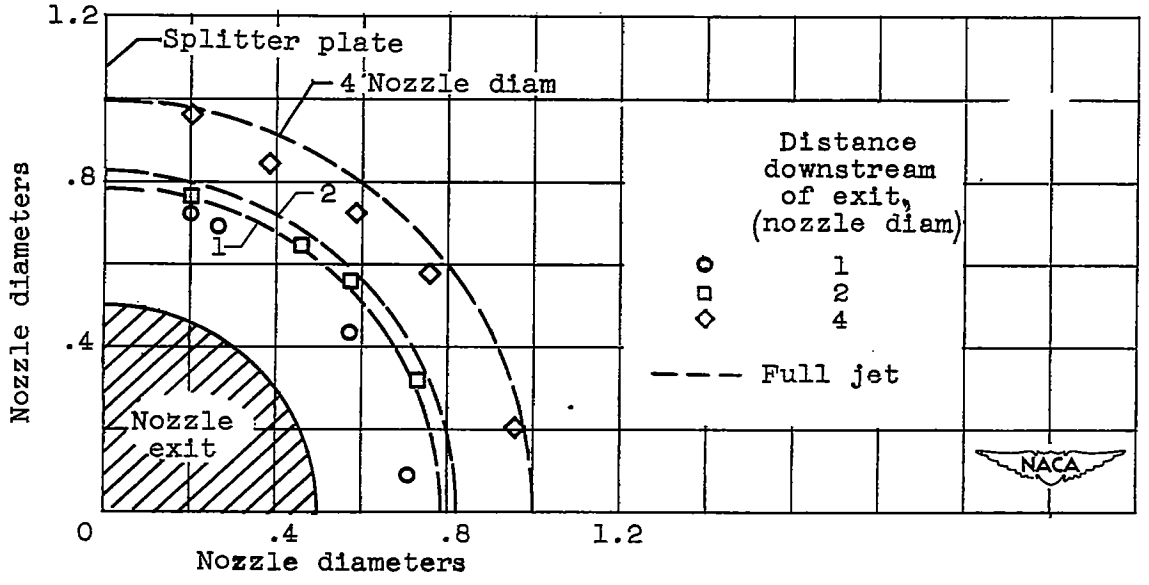

Figure 4. - Comparison of jet boundaries for full and half jets at several stations. Jet pressure ratio, P_j/p_a, 4.6.

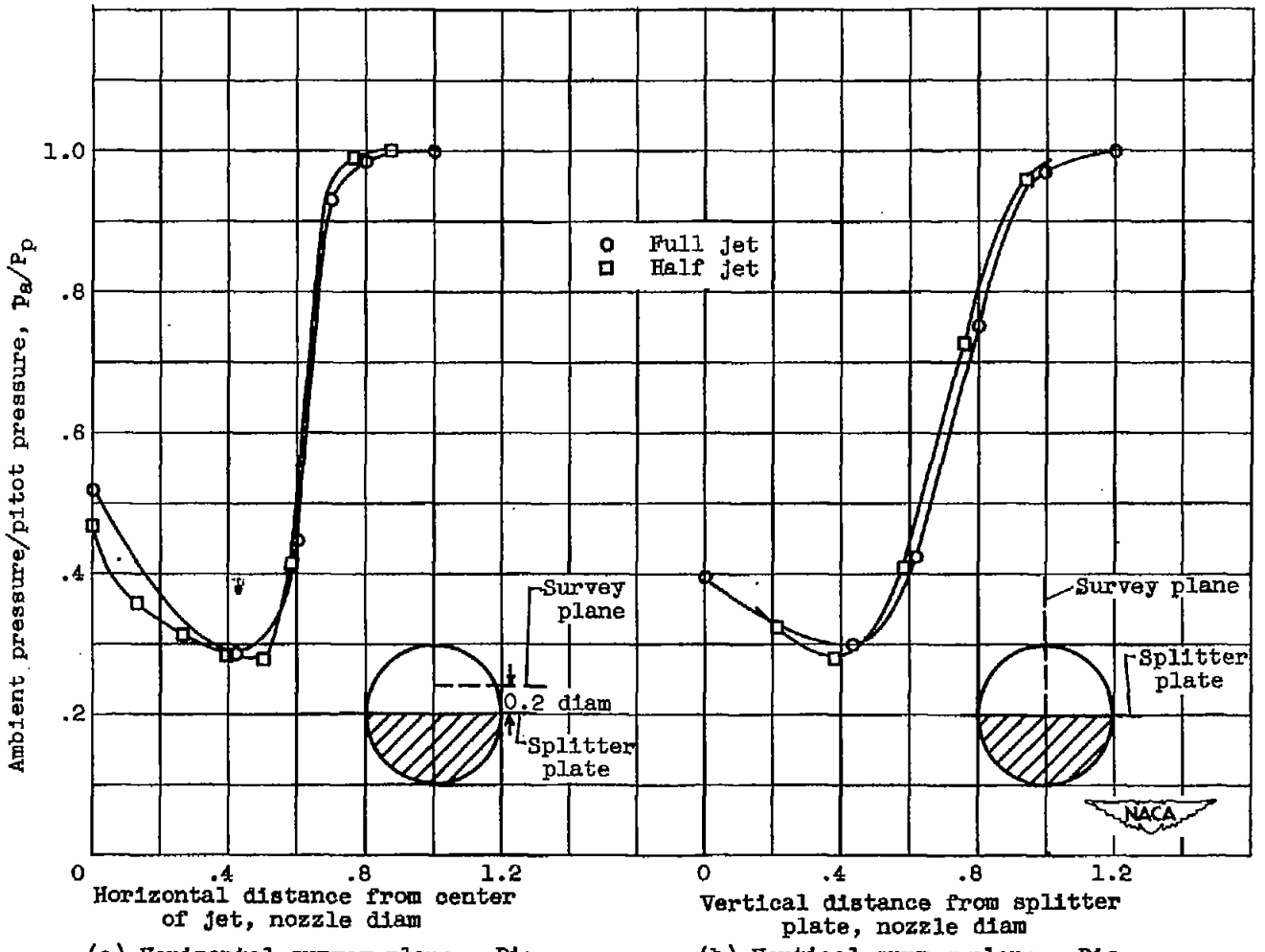

(a) Horizontal survey plane. Distance from nozzle exit, 1 nozzle diameter.

(b) Vertical survey plane. Distance from nozzle exit, 4 nozzle diameter.

Figure 5. - Typical pitot pressure surveys of full and half jet. Jet pressure ratio, P_j/p_a, 4.6.

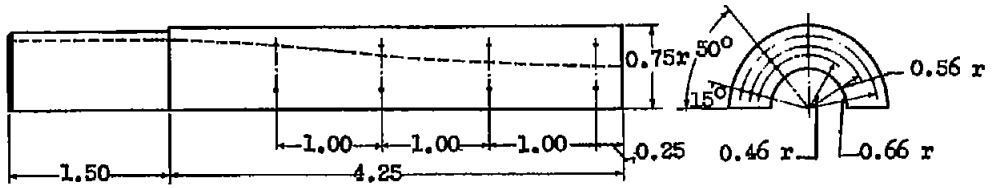

(a) Cylindrical afterbody.

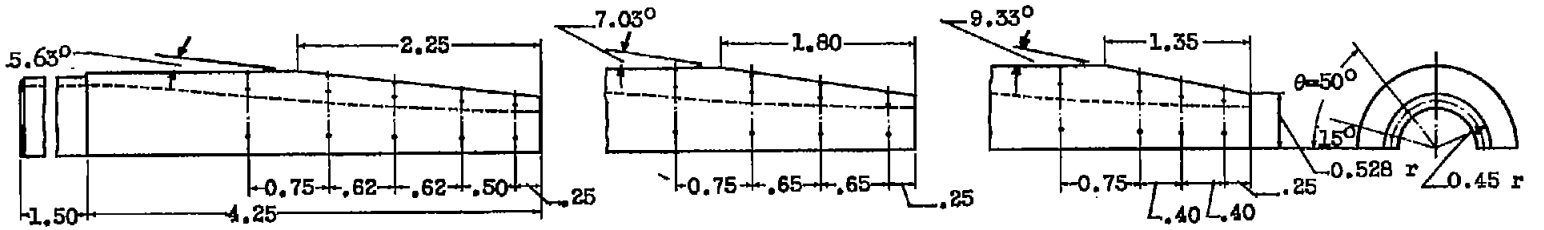

(b) Conical boattails. Base to body diameter ratio D_b/D_m, 0.704.

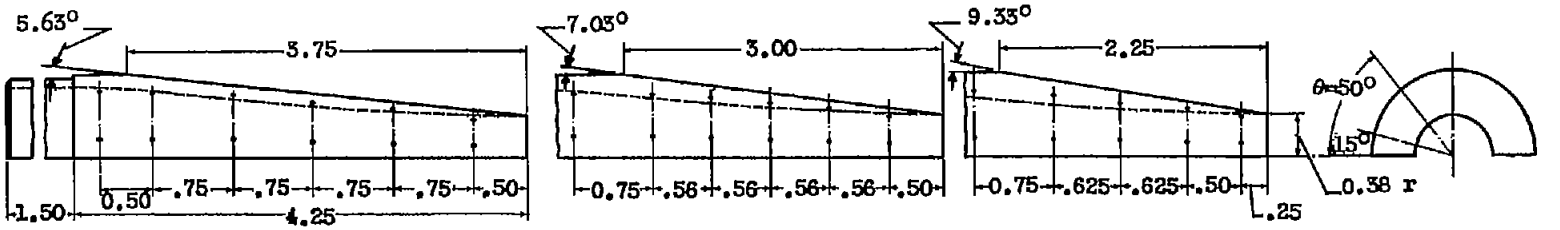

(c) Conical boattails. Base to body diameter ratio D_b/D_m, 0.506.

Figure 6. - Sketch of boattail configurations investigated showing external dimensions and location of static orifices. All dimensions in inches.

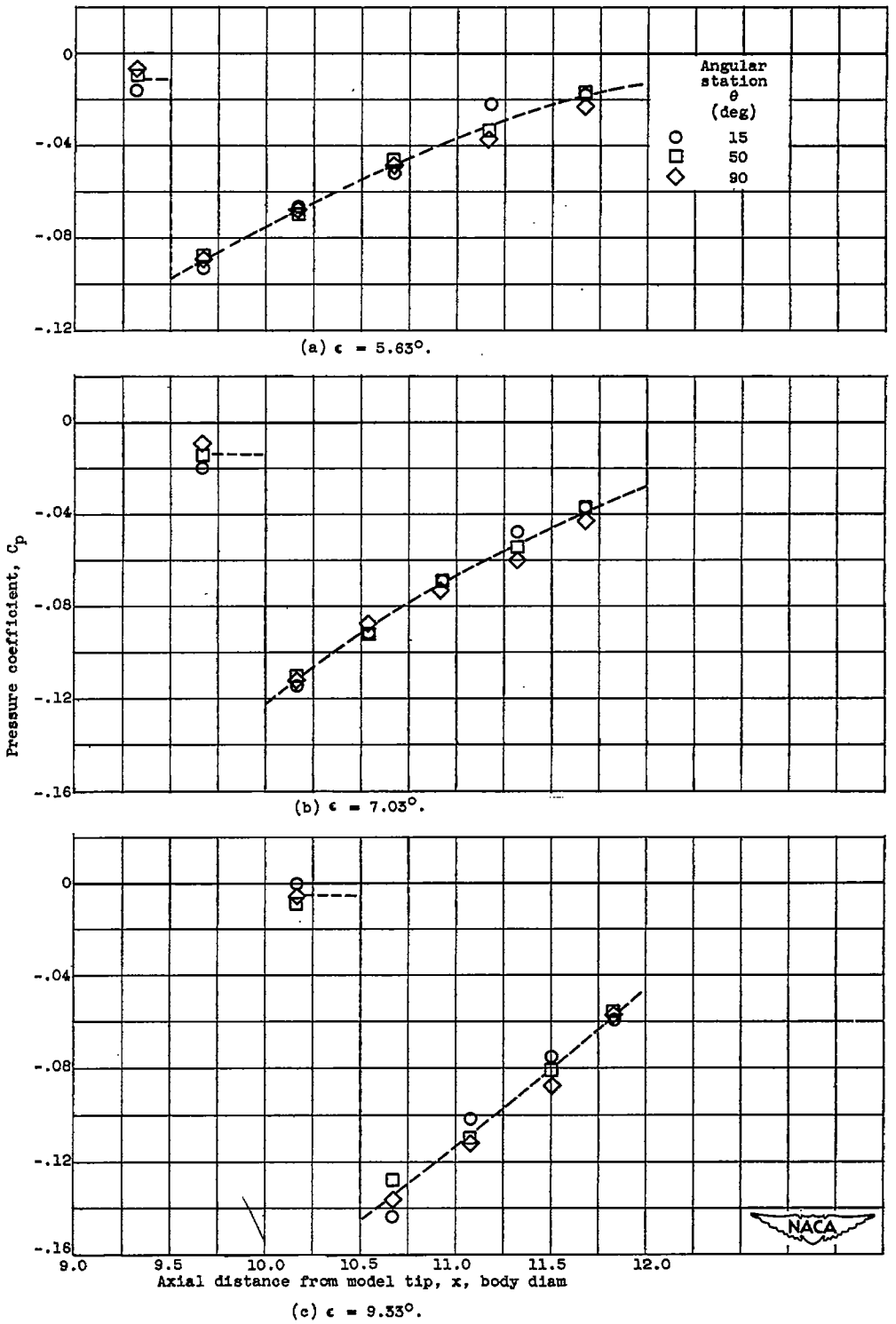

(a) ϵ = 5.63°.

(b) ϵ = 7.03°.

(c) ϵ = 9.33°.

Figure 7. - Variation of pressure coefficient with axial station for completely boattailed configurations with various boattail angles ϵ. Angle of attack α, 0°; base to body diameter ratio D_b/D_m, 0.506; no jet flow.

2228

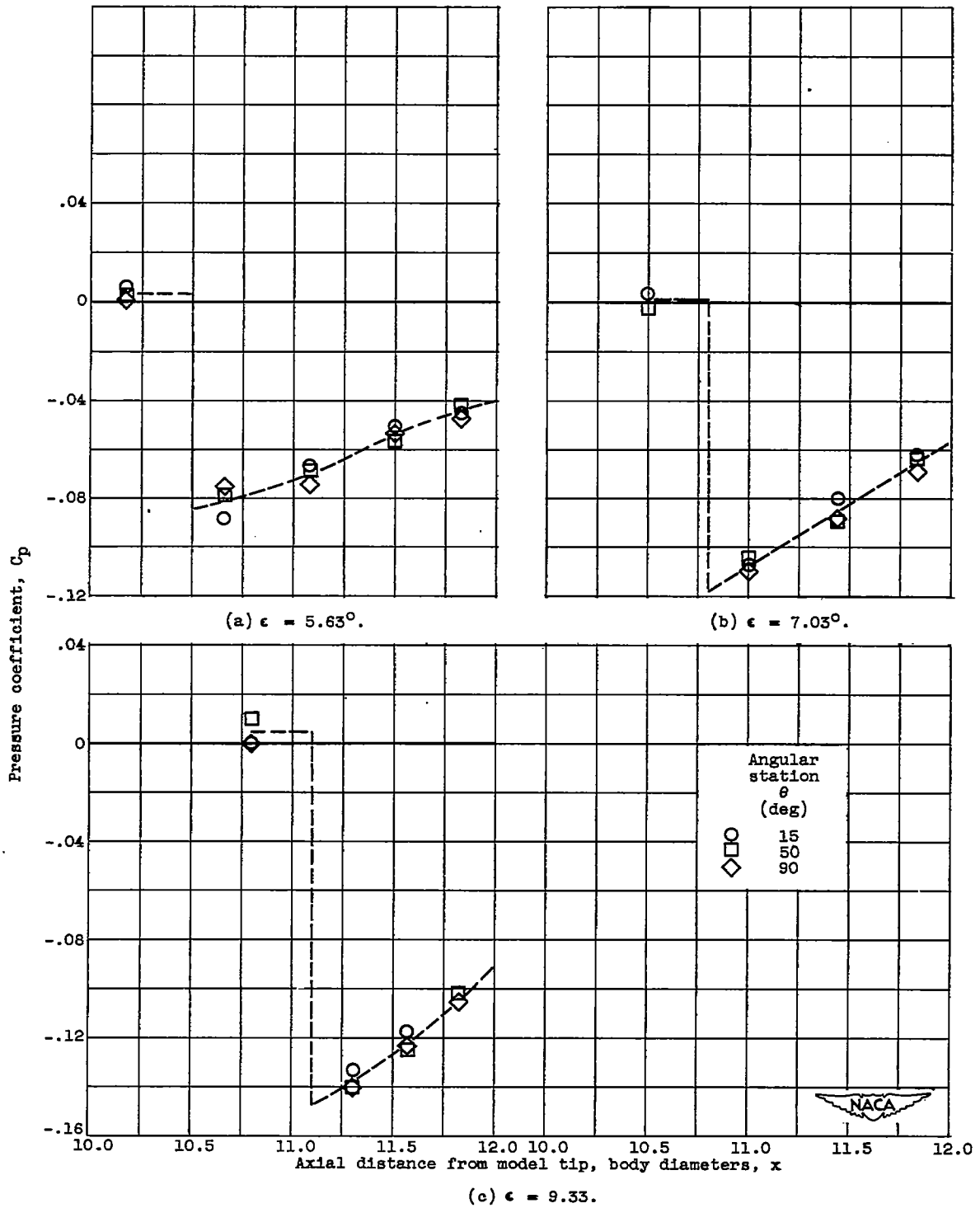

Figure 8. - Variation of pressure coefficient with axial station for incompletely boattailed configurations. Angle of attack α, 0°; base to body diameter ratio D_b/D_m, 0.704; no jet flow.

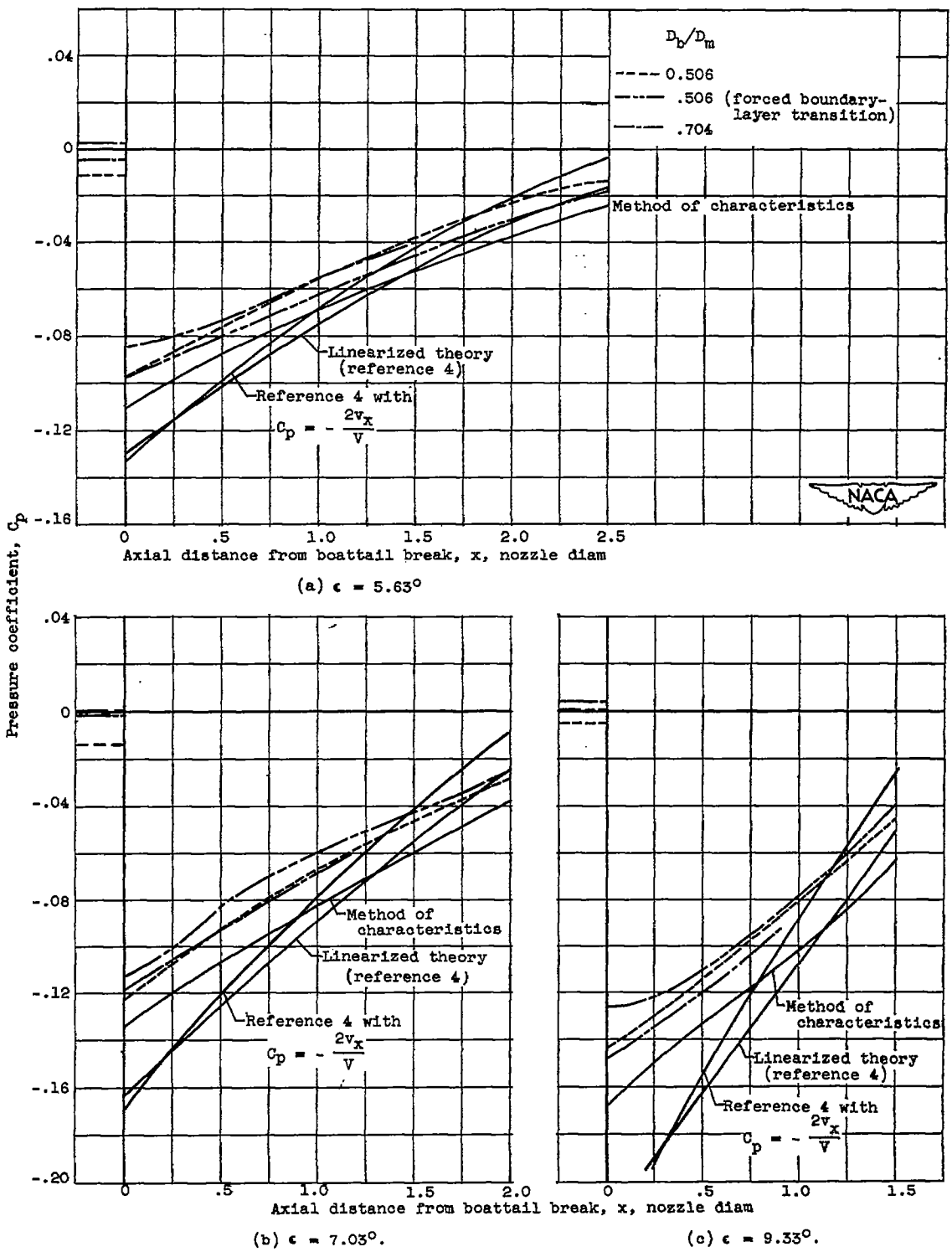

Figure 9. - Mean variation of pressure coefficient with axial distance from boattail break for various boattail angles ϵ compared with linearized and characteristics theory. Angle of attack α, 0°; base to body diameter ratio D_b/D_m, 0.506 and 0.704.

2228

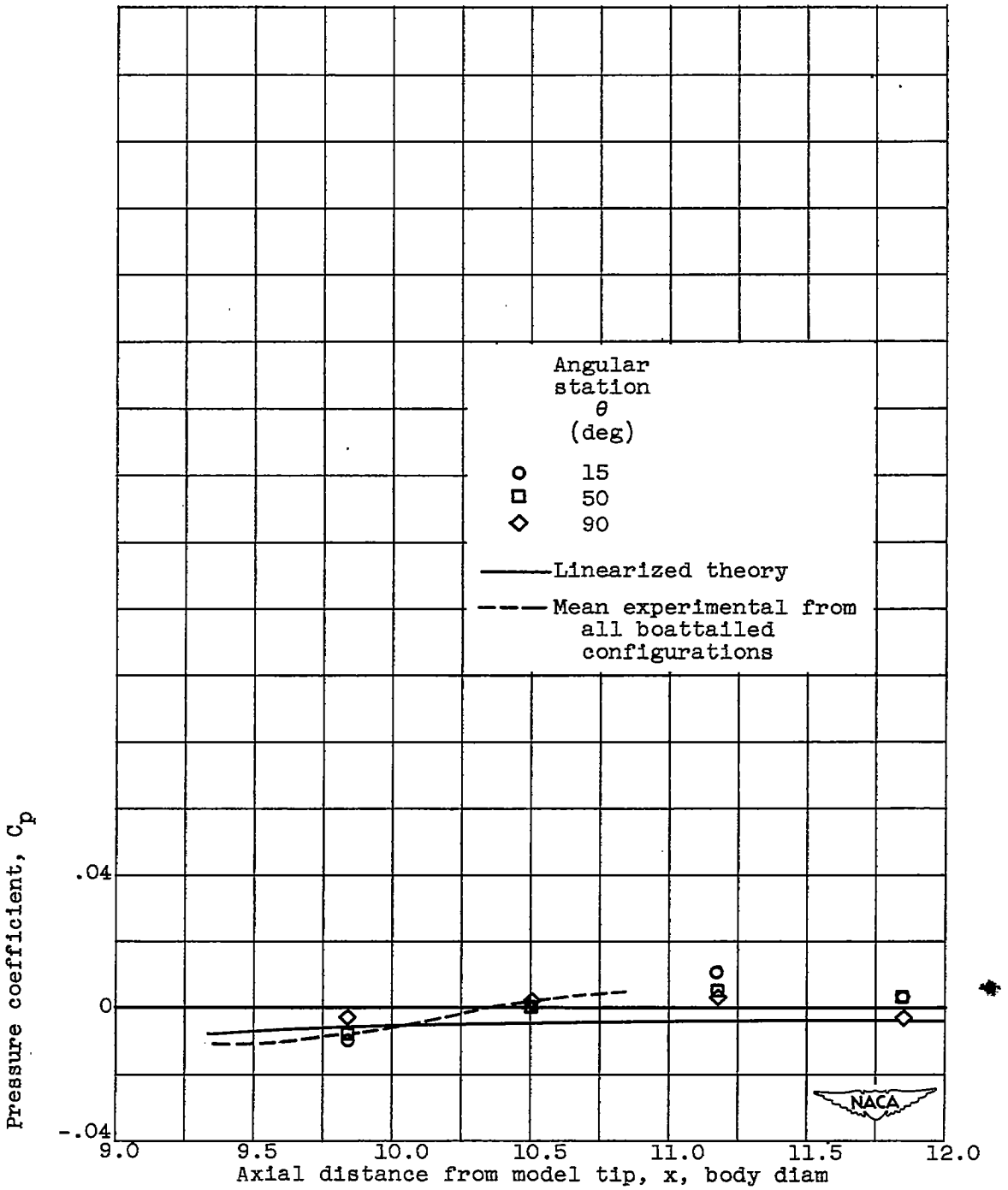

Figure 10. - Variation of pressure coefficient with axial distance from model tip for cylindrical afterbody compared with linearized theory and mean experimental data from all boattail configurations.

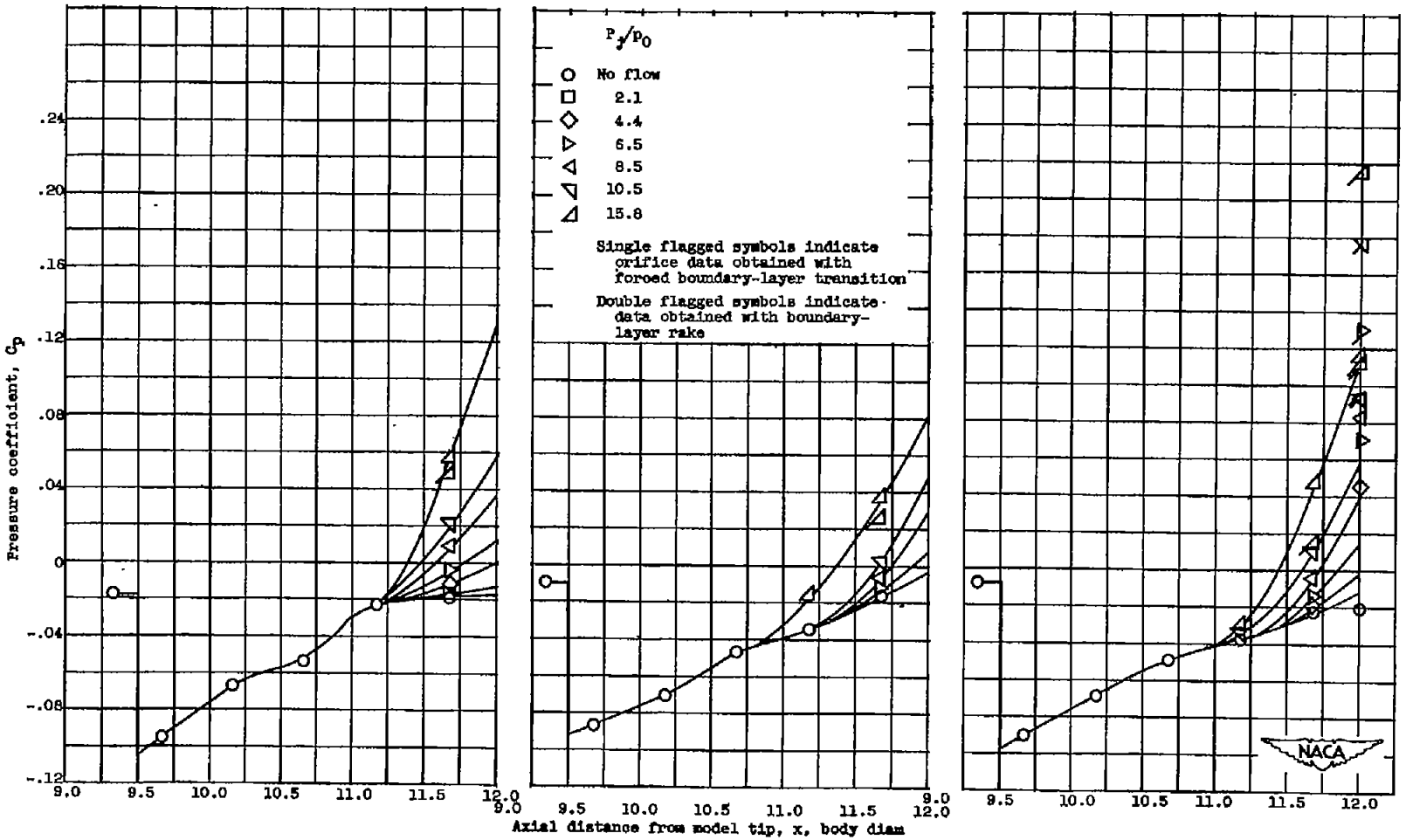

(a) θ = 15°. (b) θ = 50°. (c) θ = 80°.

Figure 11. - Variation of pressure coefficient with axial station for various values of jet pressure ratio P_j/p_0 and angular station θ. Angle of attack α, 0°; boattail angle ϵ, 5.65°; base to body diameter ratio D_b/D_m, 0.508.

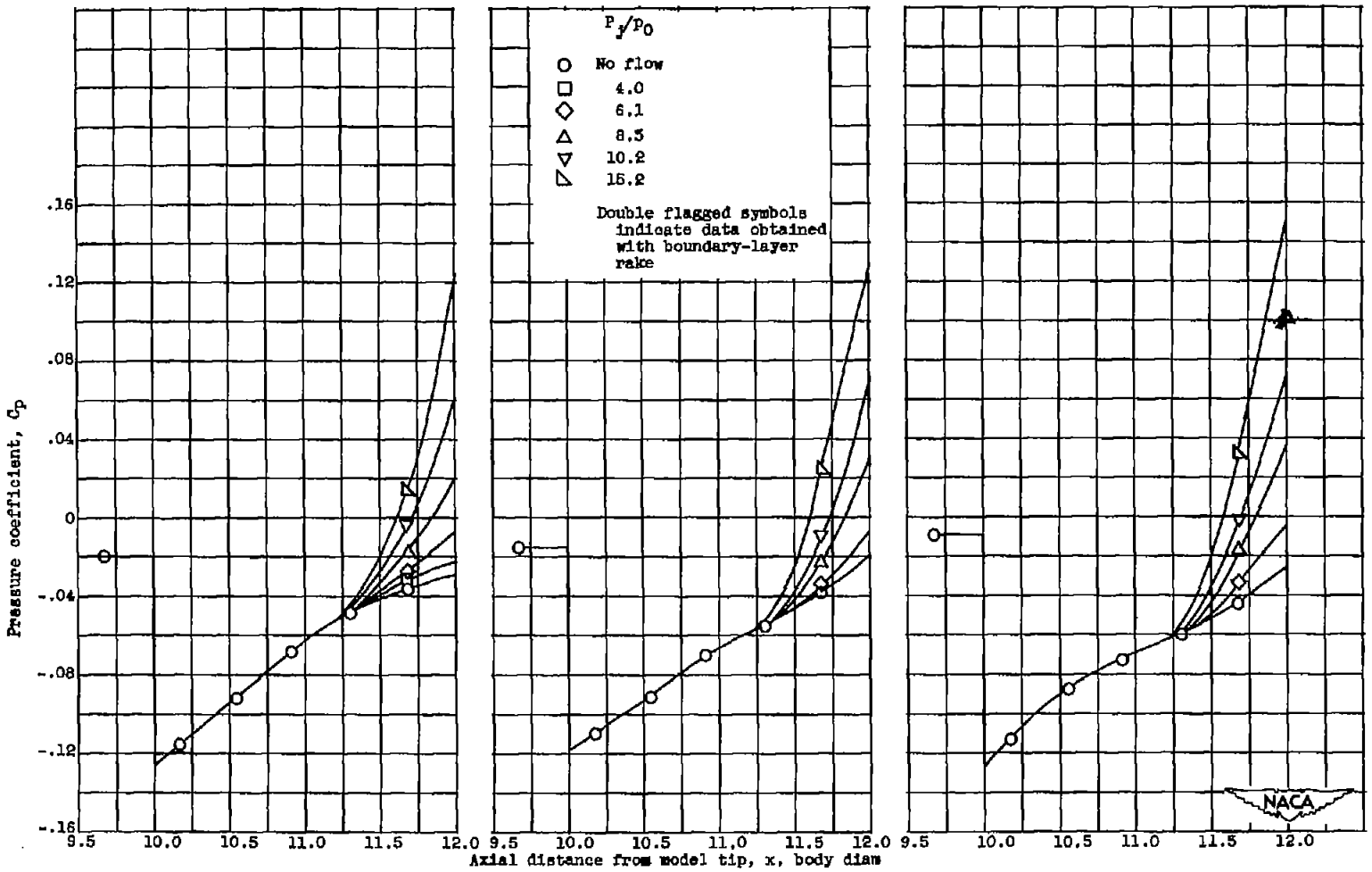

(a) $\theta = 15^\circ$. (b) $\theta = 50^\circ$. (c) $\theta = 90^\circ$.

Figure 12. - Variation of pressure coefficient with axial station for various values of jet pressure ratio P_j/p_0 and angular station θ. Angle of attack α, 0°; boattail angle ϵ, 7.03°; base to body diameter ratio D_b/D_m, 0.506.

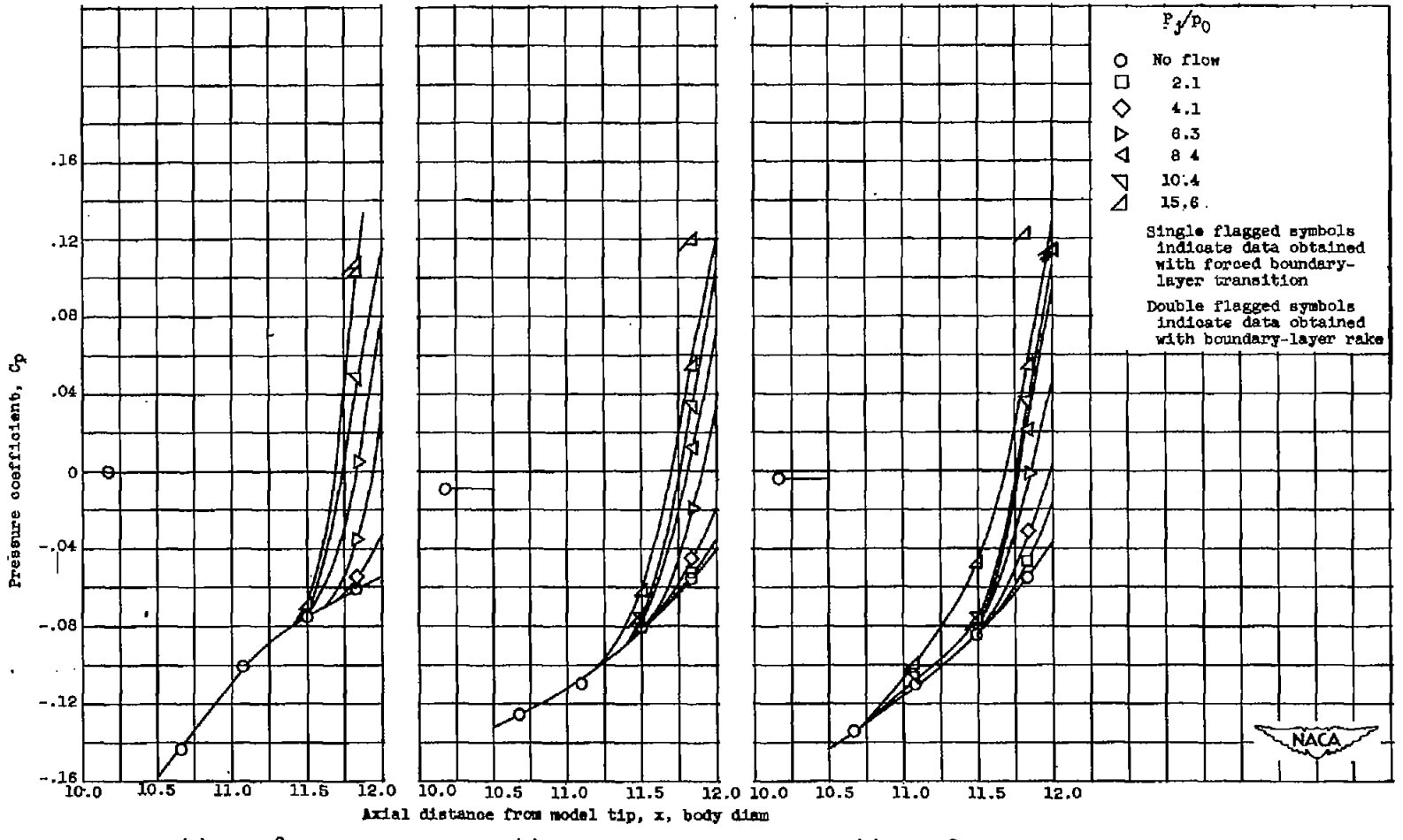

(a) $\theta = 15^\circ$. (b) $\theta = 50^\circ$. (c) $\theta = 90^\circ$.

Figure 13. - Variation of pressure coefficient with axial station for various values of jet pressure ratio P_j/p_0 and angular station θ. Angle of attack α, 0°; boattail angle ϵ, 9.33°; base to body diameter ratio D_b/D_m, 0.506.

2228

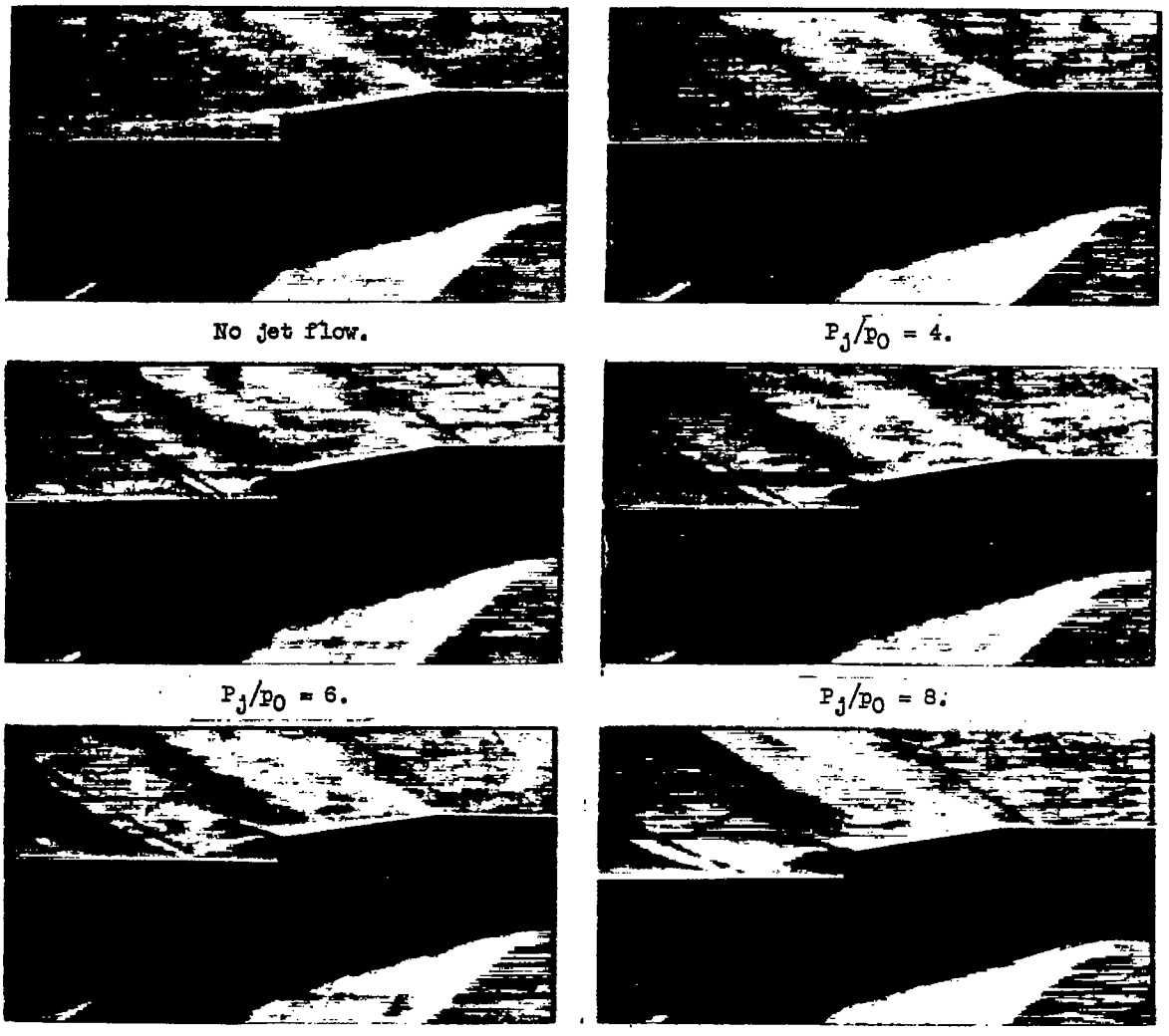

(a) Schlieren photographs at various jet pressure ratios P_j/p_0.

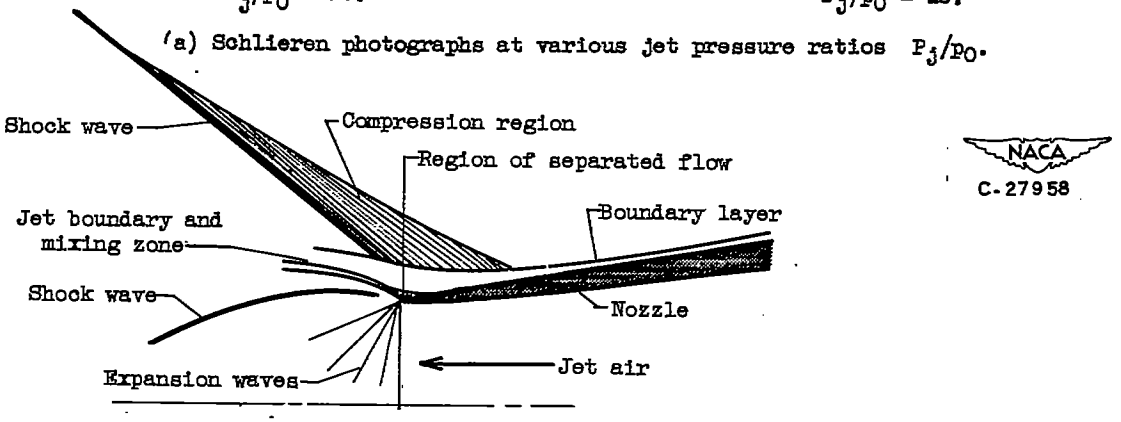

(b) Sketch at jet pressure ratio P_j/p_0 of approximately 10.

Figure 14. - Schlieren photographs and sketch of flow in base region for completely boattailed body. Mach number M, 1.91; angle of attack α, 0°; boattail angle ϵ, 9.33°; base to body diameter ratio D_b/D_m, 0.506.

ϵ = 9.33°.

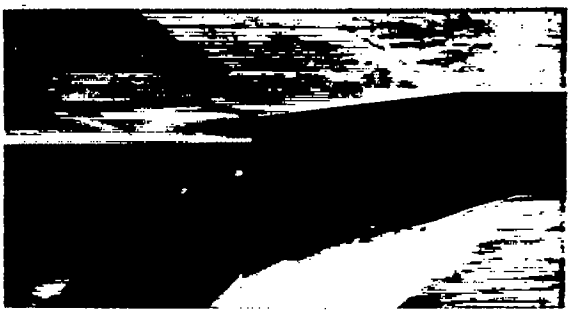

ϵ = 7.03°.

ϵ = 5.63°.

Figure 15. - Schlieren photographs of completely boattailed bodies with various boattail angles ϵ. Angle of attack α, 0°; base to body diameter ratio D_b/D_m, 0.506; jet pressure ratio P_j/p_0, 15.

No jet.

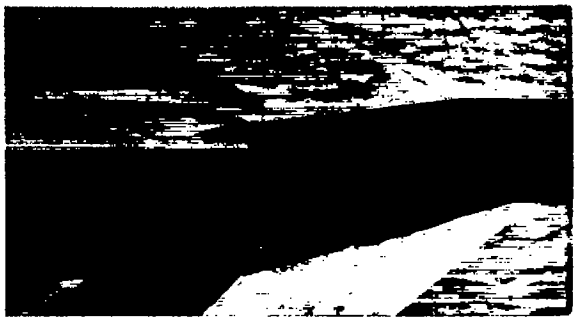

P_j/p_0 = 10.

Figure 16. - Schlieren photographs of completely boattailed bodies with artificially induced turbulence near nose of model. Angle of attack α, 0°; boattail angle ϵ, 7.03; base to body diameter ratio D_b/D_m, 0.506.

2228

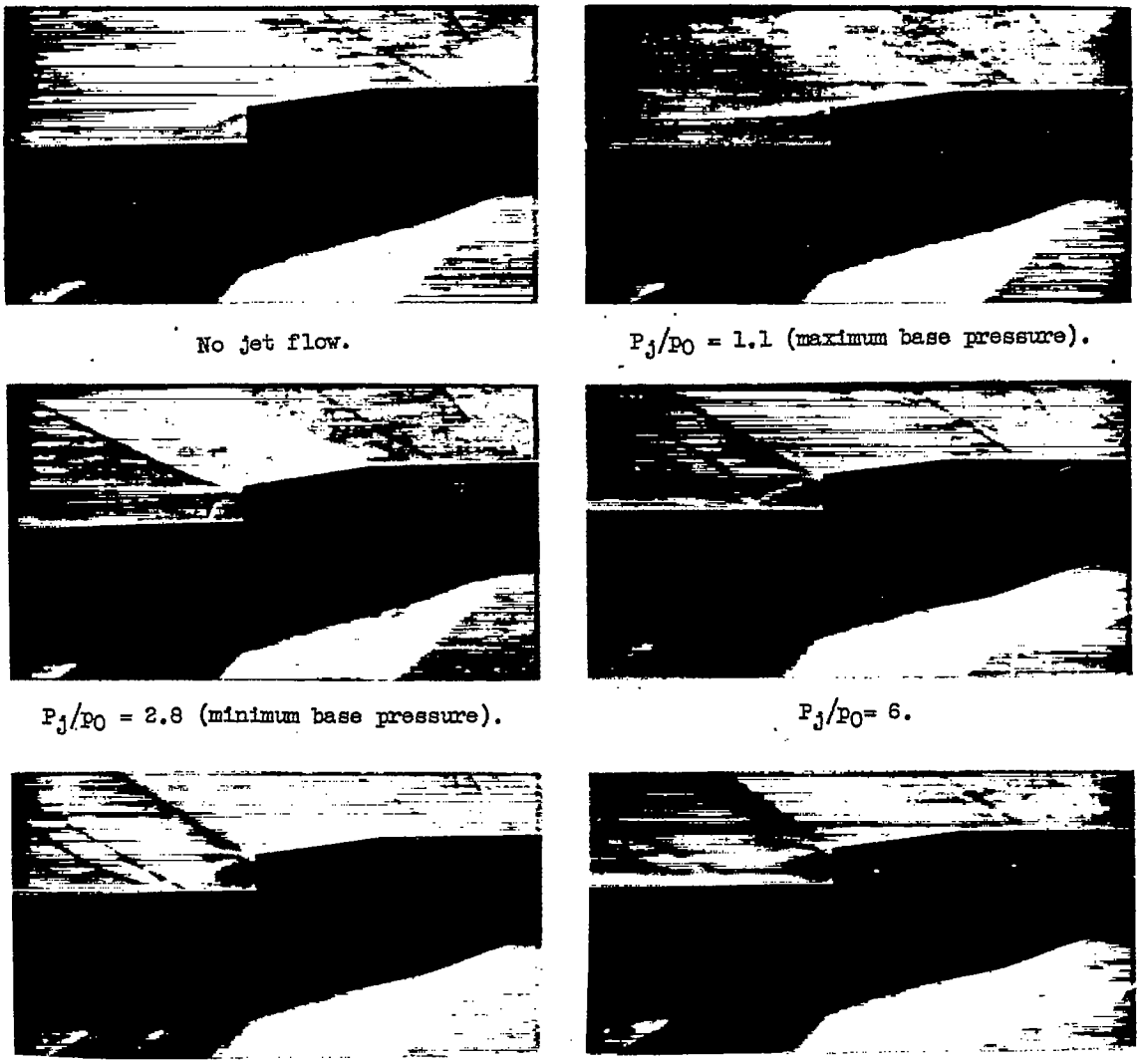

(a) Schlieren photographs at various jet pressure ratios P_j/p_0.

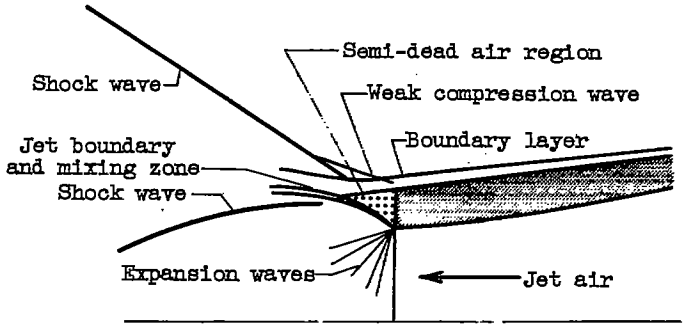

(b) Sketch at jet pressure ratio P_j/p_0 of approximately 10.

Figure 17. - Schlieren photographs and sketch of flow in base region for incompletely boattailed body. Mach number M, 1.91; angle of attack α, 0°; boattail angle ϵ, 7.03°; base to body diameter ratio D_b/D_m, 0.704.

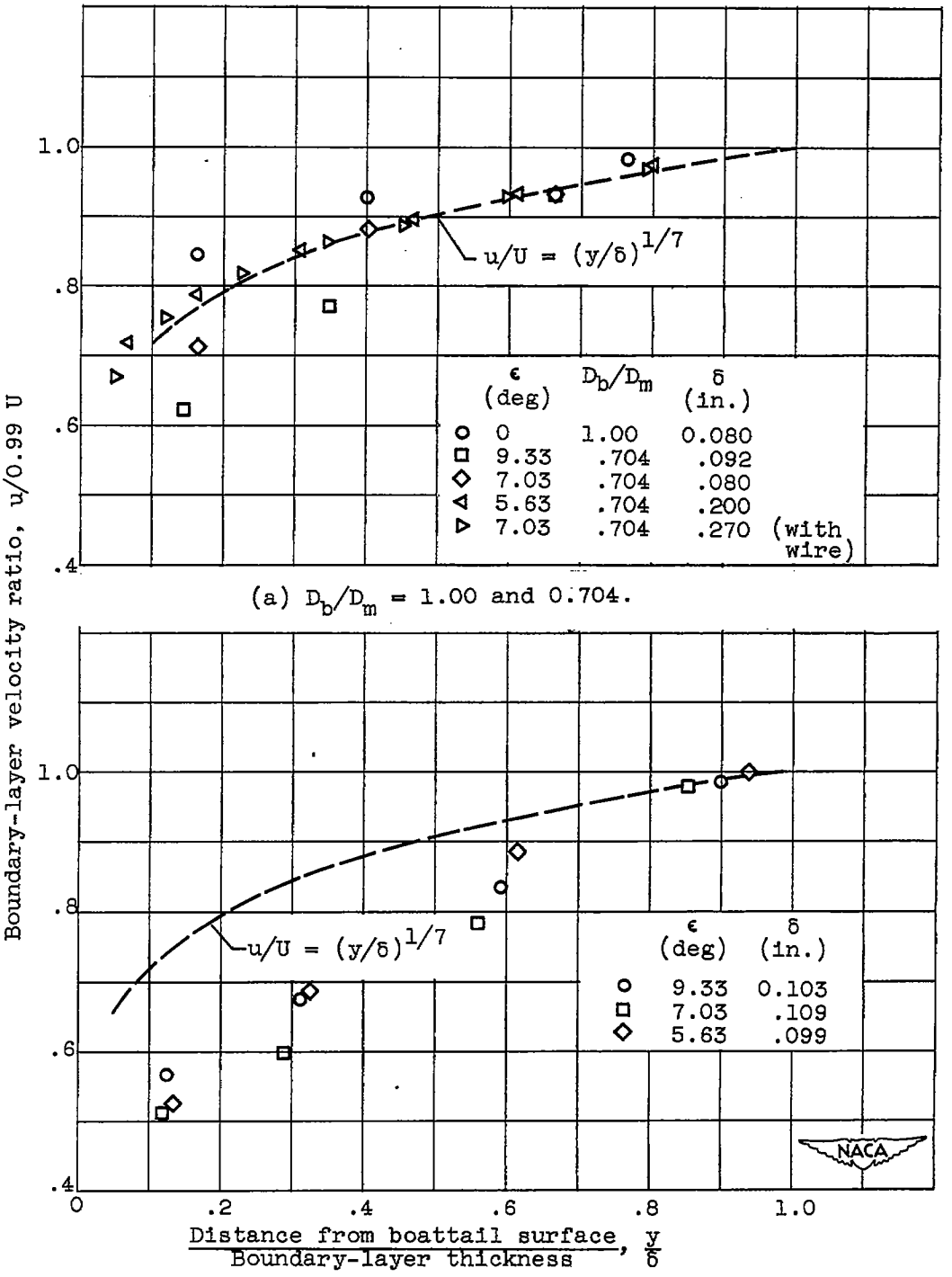

Figure 18. - Boundary-layer profiles at base of boattails. Angle of attack α, 0°; angular station θ, 90°; no jet flow.

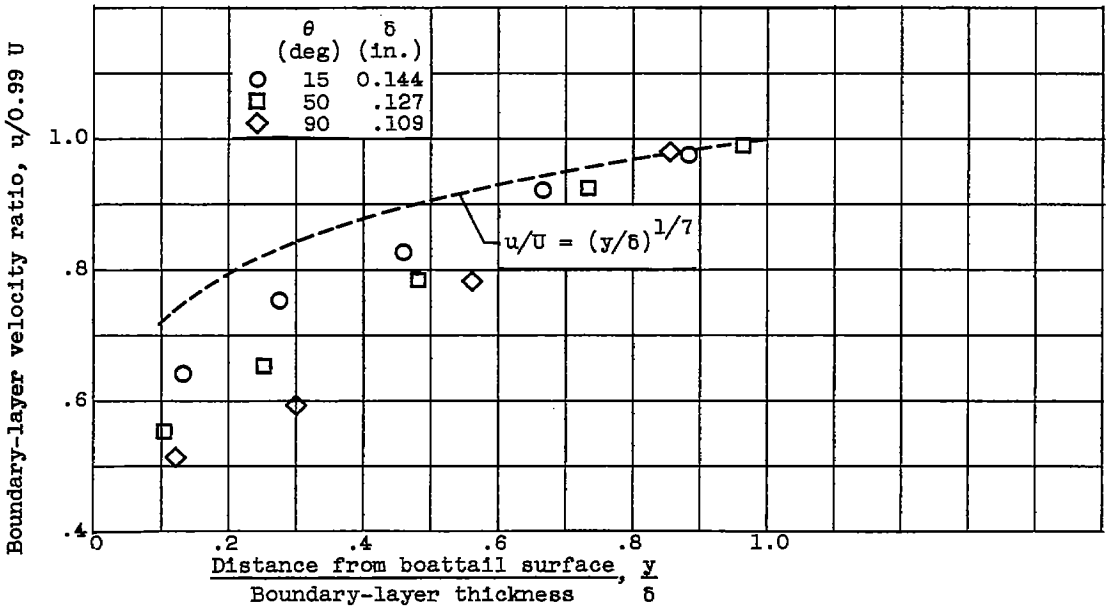

Figure 19. - Boundary-layer profiles at base of boattail. Angle of attack α, 0°; boattail angle ϵ, 7.03°; base to body diameter ratio D_b/D_m, 0.506; no jet flow.

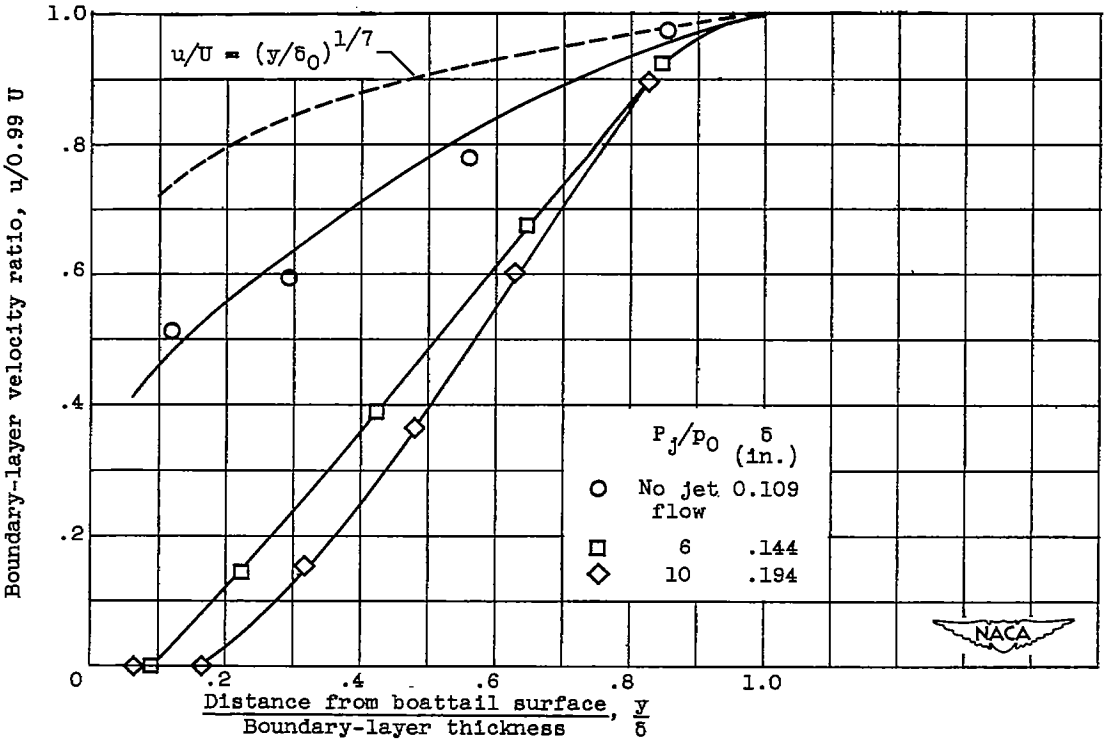

Figure 20. - Boundary-layer profiles at base of completely boattailed body for several jet pressure ratios P_j/p_0. Angle of attack α, 0°; boattail angle ϵ, 7.03°; base to body diameter ratio D_b/D_m, 0.506; angular station θ, 90°.

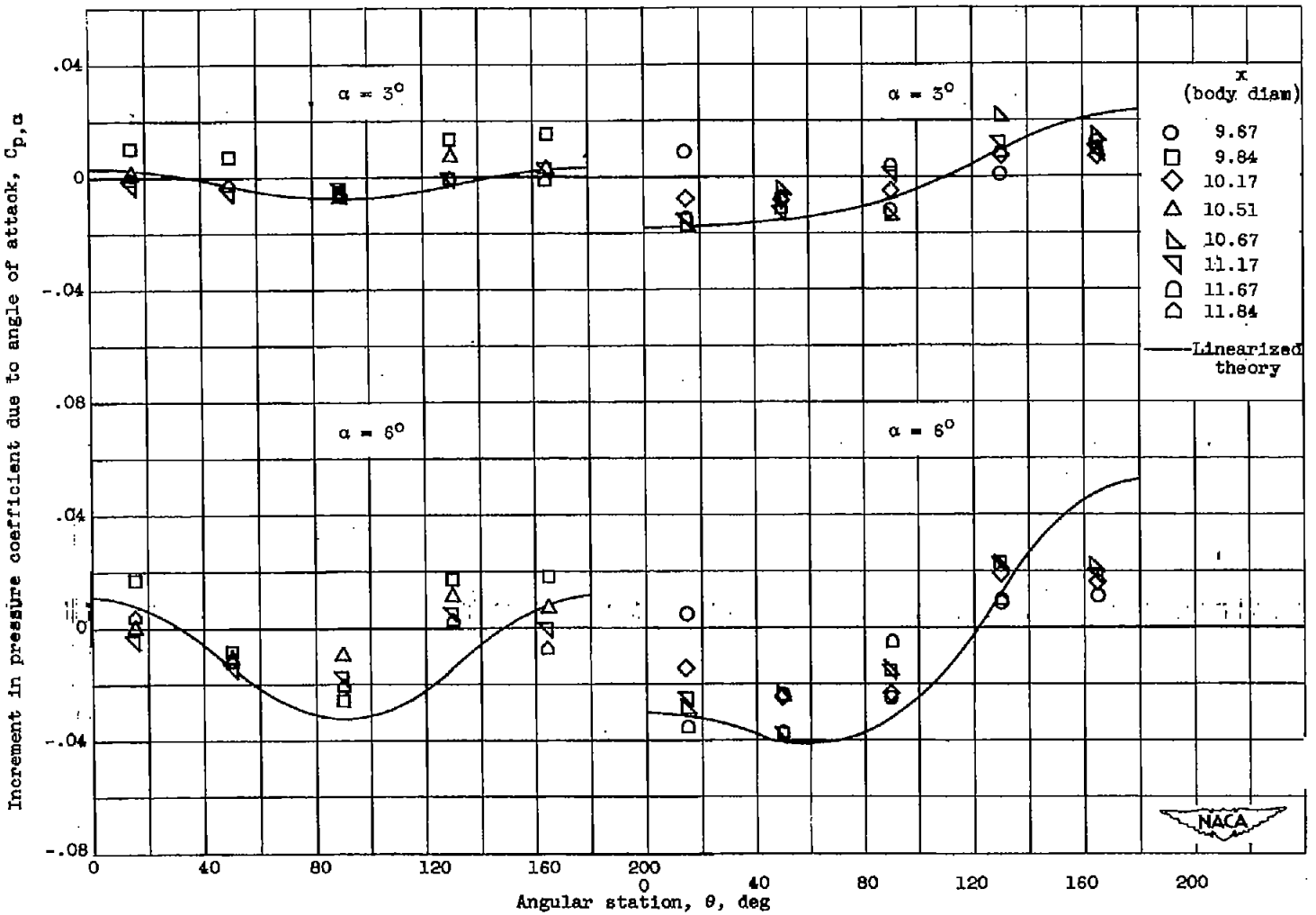

(a) $\epsilon = 0^\circ$; $D_b/D_m = 1.00$.

(b) $\epsilon = 5.63^\circ$; $D_b/D_m = 0.506$.

Figure 21. - Circumferential variation of increment in pressure coefficient due to angle of attack α at various axial stations x for various boattail angles ϵ and base to body diameter ratios D_b/D_m.

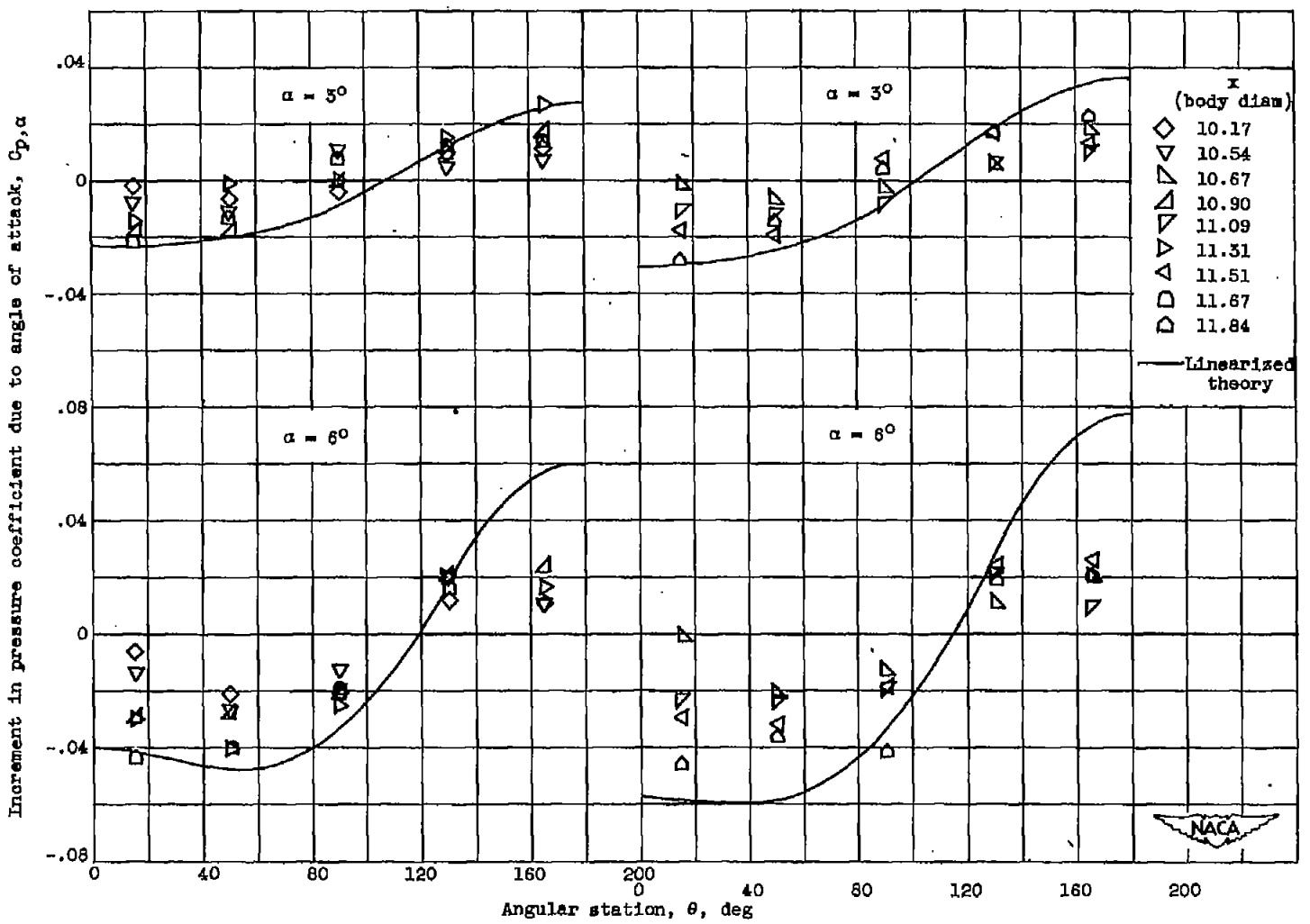

(c) ϵ = 7.03°; D_b/D_m = 0.506.

(d) ϵ = 9.33°; D_b/D_m = 0.506.

Figure 21. - Concluded. Circumferential variation of increment in pressure coefficient due to angle of attack α at various axial stations x for various boattail angles ϵ and base to body diameter ratios D_b/D_m.

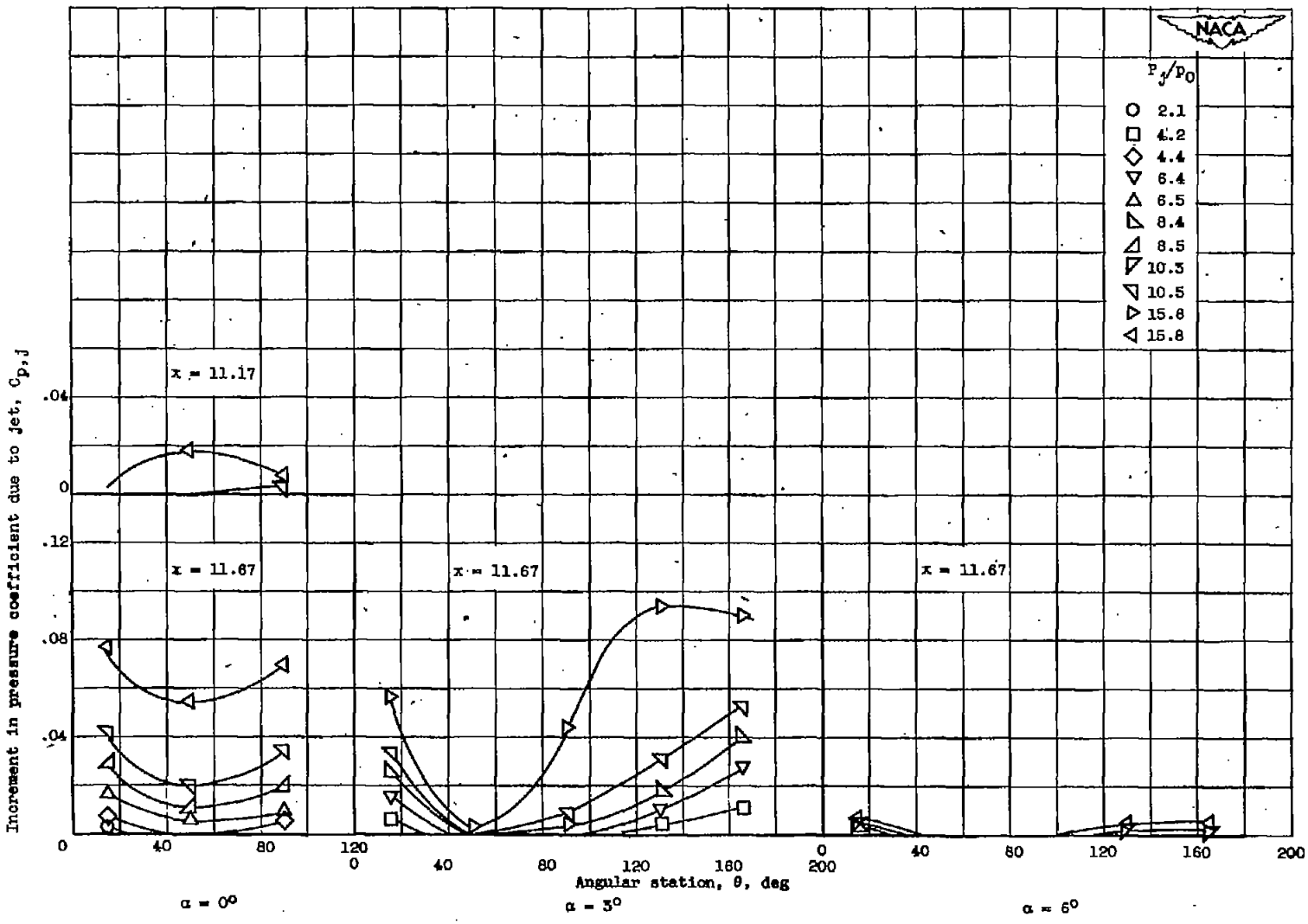

(a) $\epsilon = 5.65°$.

Figure 22. - Variation of increment in pressure coefficient due to jet with angular station for various values of jet pressure ratio P_j/p_0, axial station x, angle of attack α, and boattail angle ε. Base to body diameter ratio D_b/D_m, 0.506.

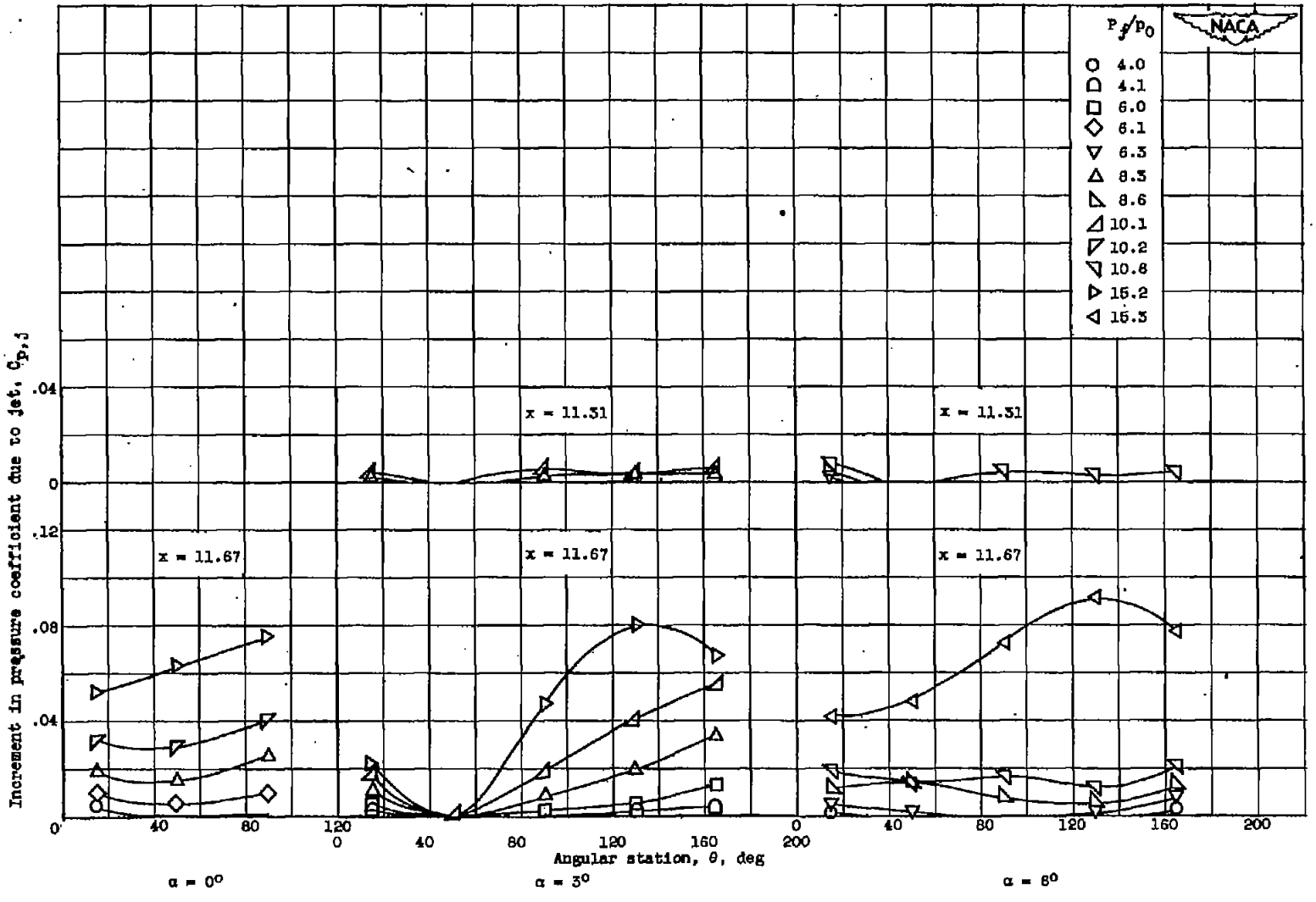

(b) ϵ = 7.05°.

Figure 22. - Continued. Variation of increment in pressure coefficient due to jet with angular station for various values of jet pressure ratio P_j/p_0, axial station x, angle of attack α, and boattail ϵ. Base to body diameter ratio D_b/D_m, 0.506

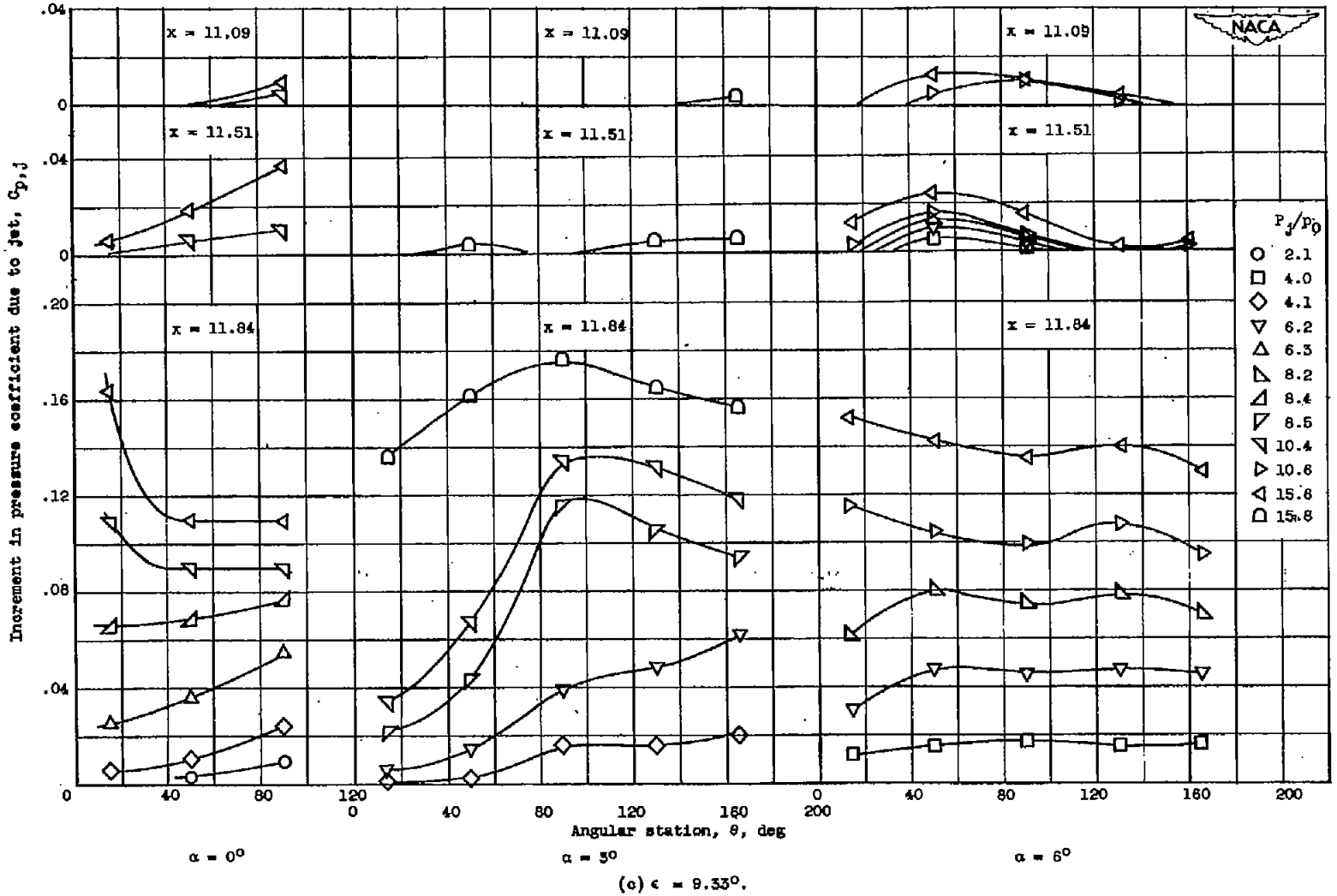

Figure 22. - Concluded. Variation of increment in pressure coefficient due to jet with angular station for various values of jet pressure ratio P_j/p_0, axial station x, angle of attack α, and boattail angle ε. base to body diameter ratio D_b/D_m, 0.506.

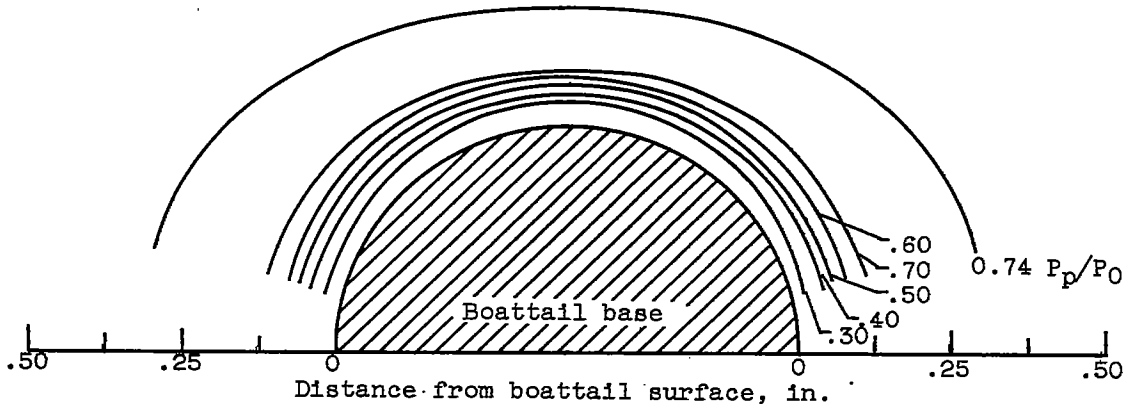

(a) $\alpha = 0^\circ$; no jet flow.

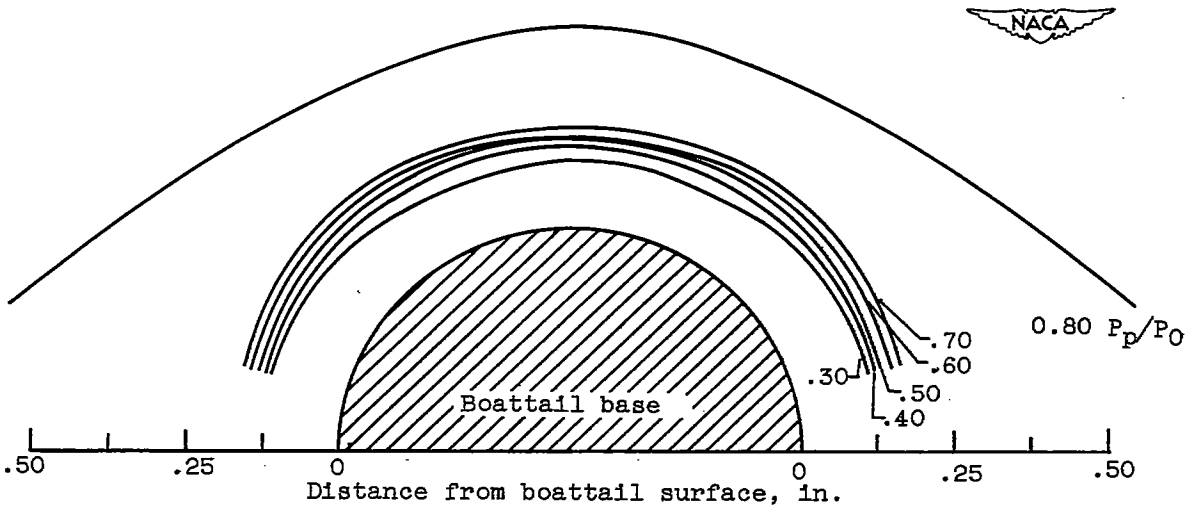

(b) $\alpha = 0^\circ$; $P_j/p_0 = 10$.

Figure 23. - Pitot pressure contours of boundary layer at base of boattail for two angles of attack α for no jet flow and jet pressure ratio P_j/p_0 of 10. Boattail angle ϵ, 7.03°; base to body diameter ratio D_b/D_m, 0.506

2228

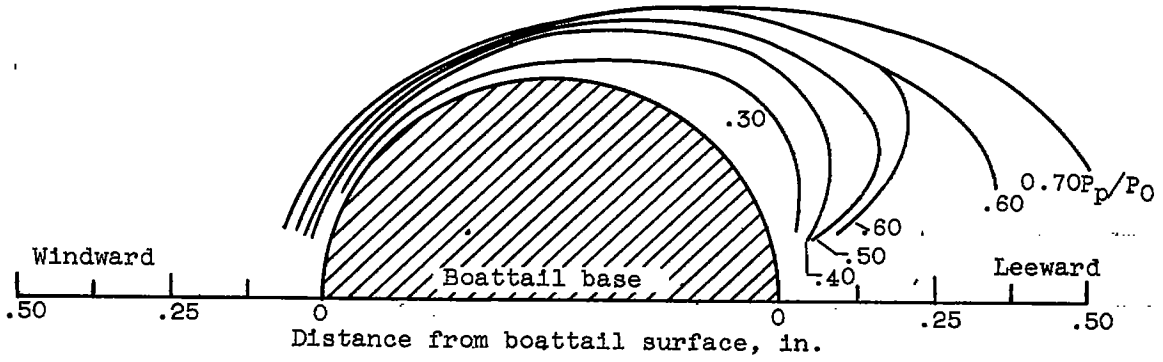

(c) $\alpha = 6^\circ$; no jet flow.

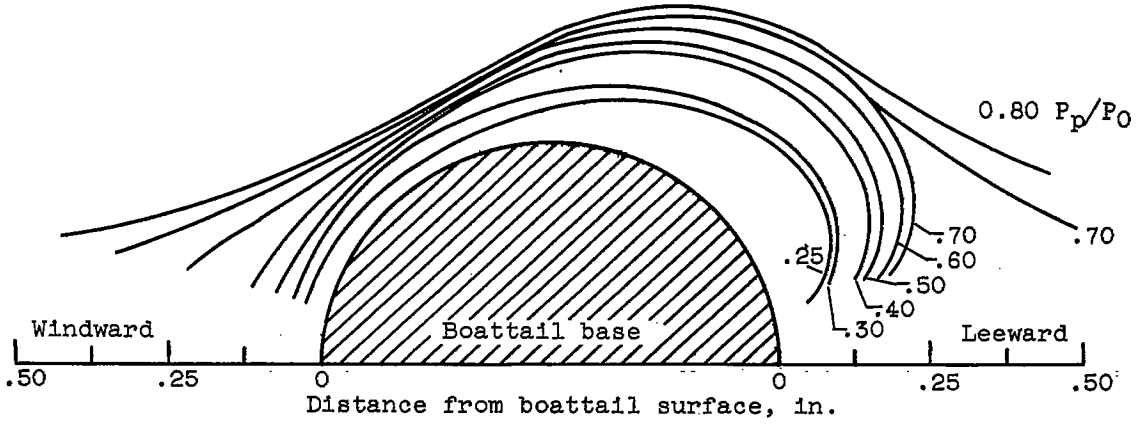

(d) $\alpha = 6^\circ$; $P_j/p_0 = 10$.

Figure 23. - Concluded. Pitot pressure contours of boundary layer at base of boattail for two angles of attack α for no jet flow and jet pressure ratio P_j/p_0 of 10. Boattail angle ϵ, 7.03°; base to body diameter ratio D_b/D_m, 0.506.

2228

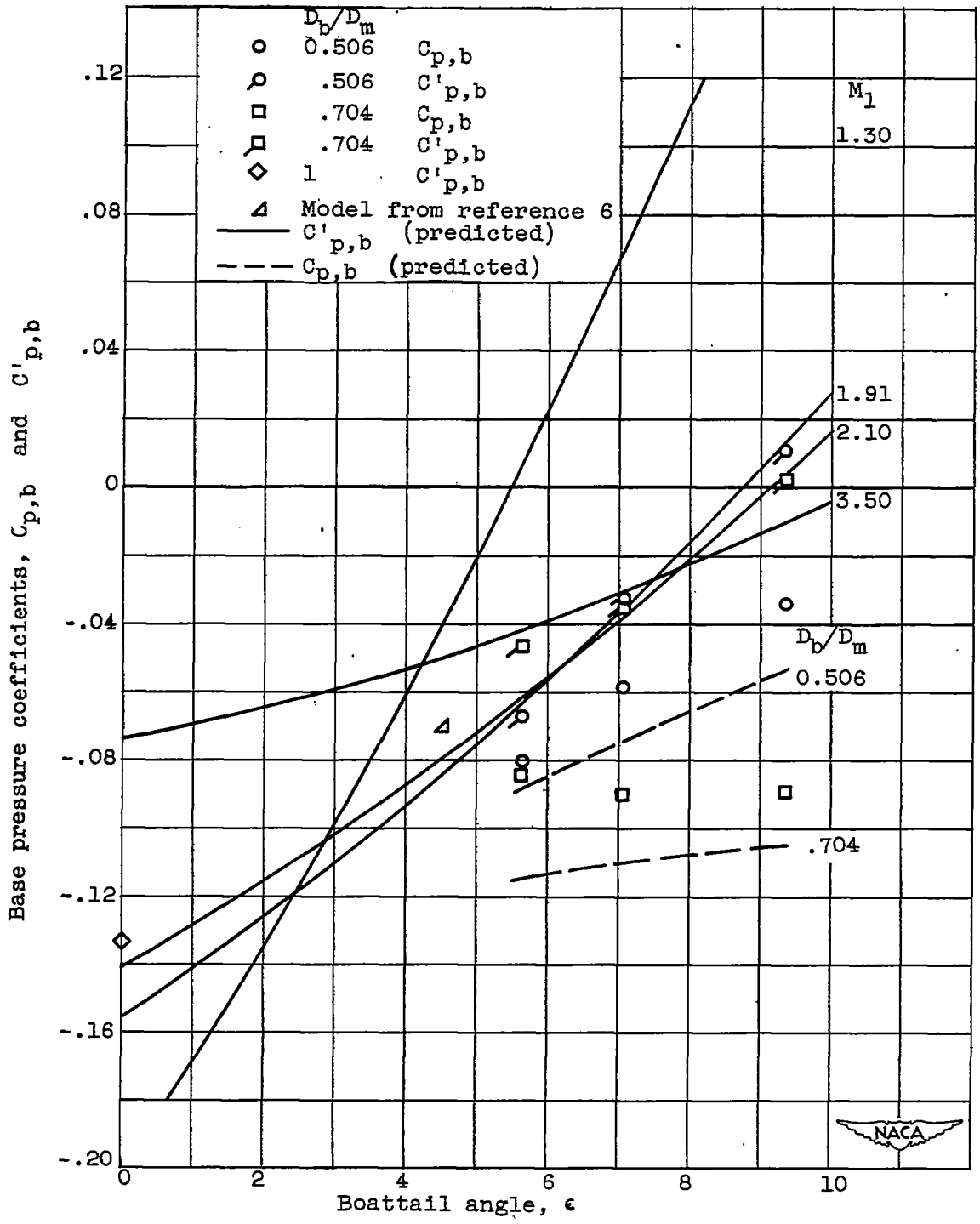

Figure 24. - Variation of base pressure coefficients with boattail angle at various Mach numbers M_1 and base to body diameter ratios D_b/D_m. Angle of attack α, 0°; no jet flow.

8222

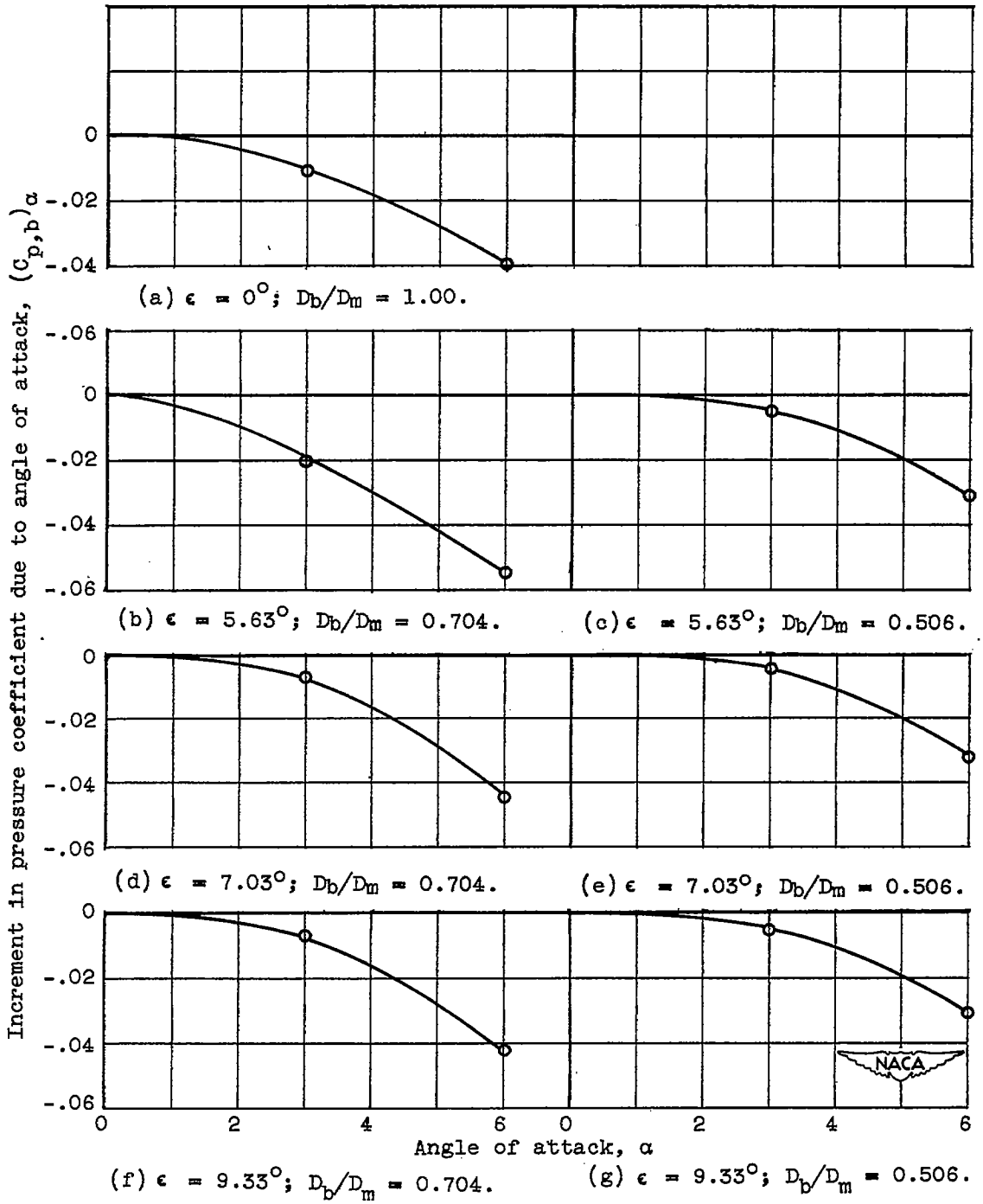

Figure 25. - Variation of experimental increment in base pressure coefficient due to angle of attack with angle of attack for boattail configurations of various values of boattail angle ϵ and base to body diameter ratio D_b/D_m.

2228

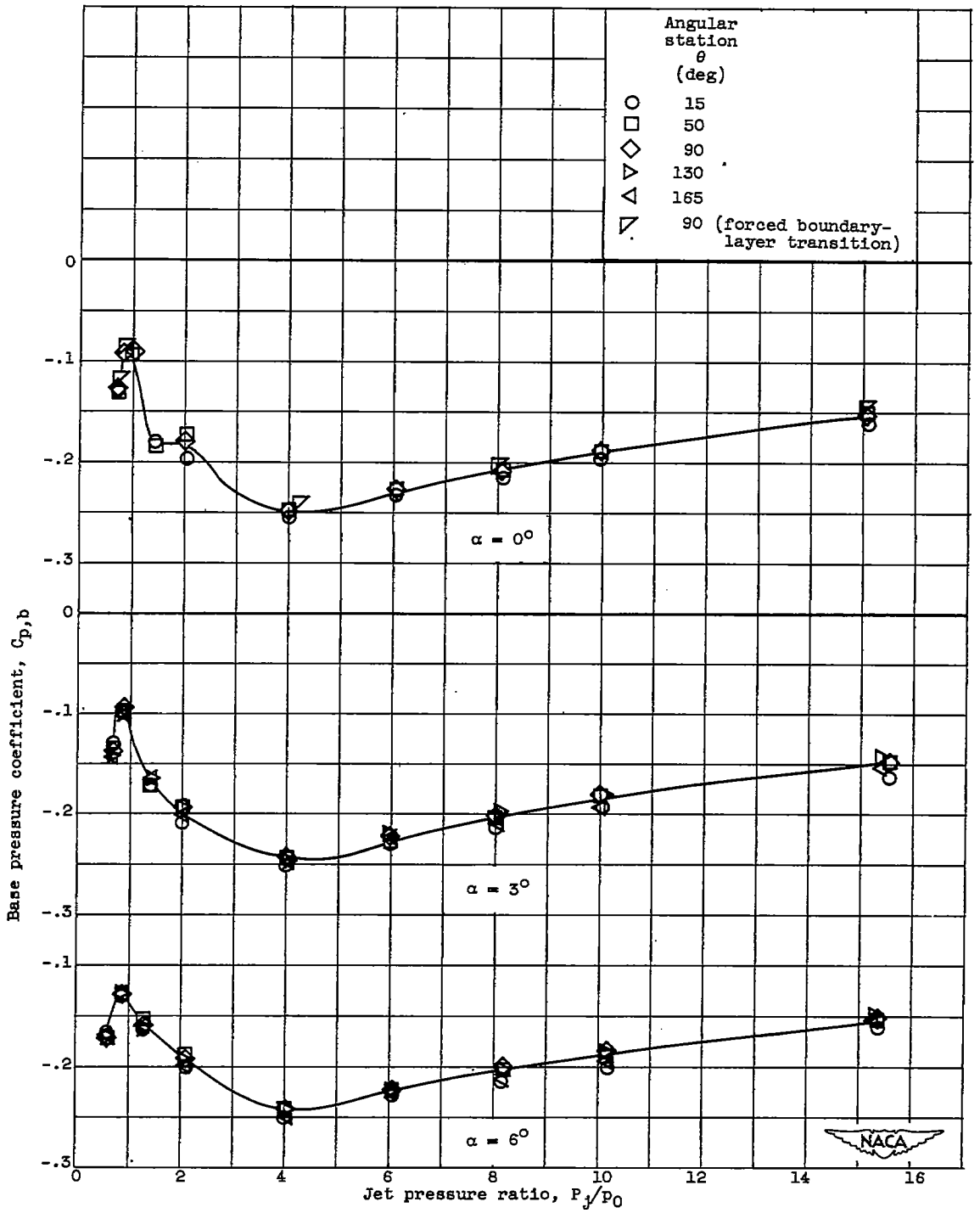

(a) $\epsilon = 0°$; $D_b/D_m = 1.00$.

Figure 26. - Variation of base pressure coefficient with jet pressure ratio for various angles of attack α, boattail angles ϵ, and base to body diameter ratios D_b/D_m.

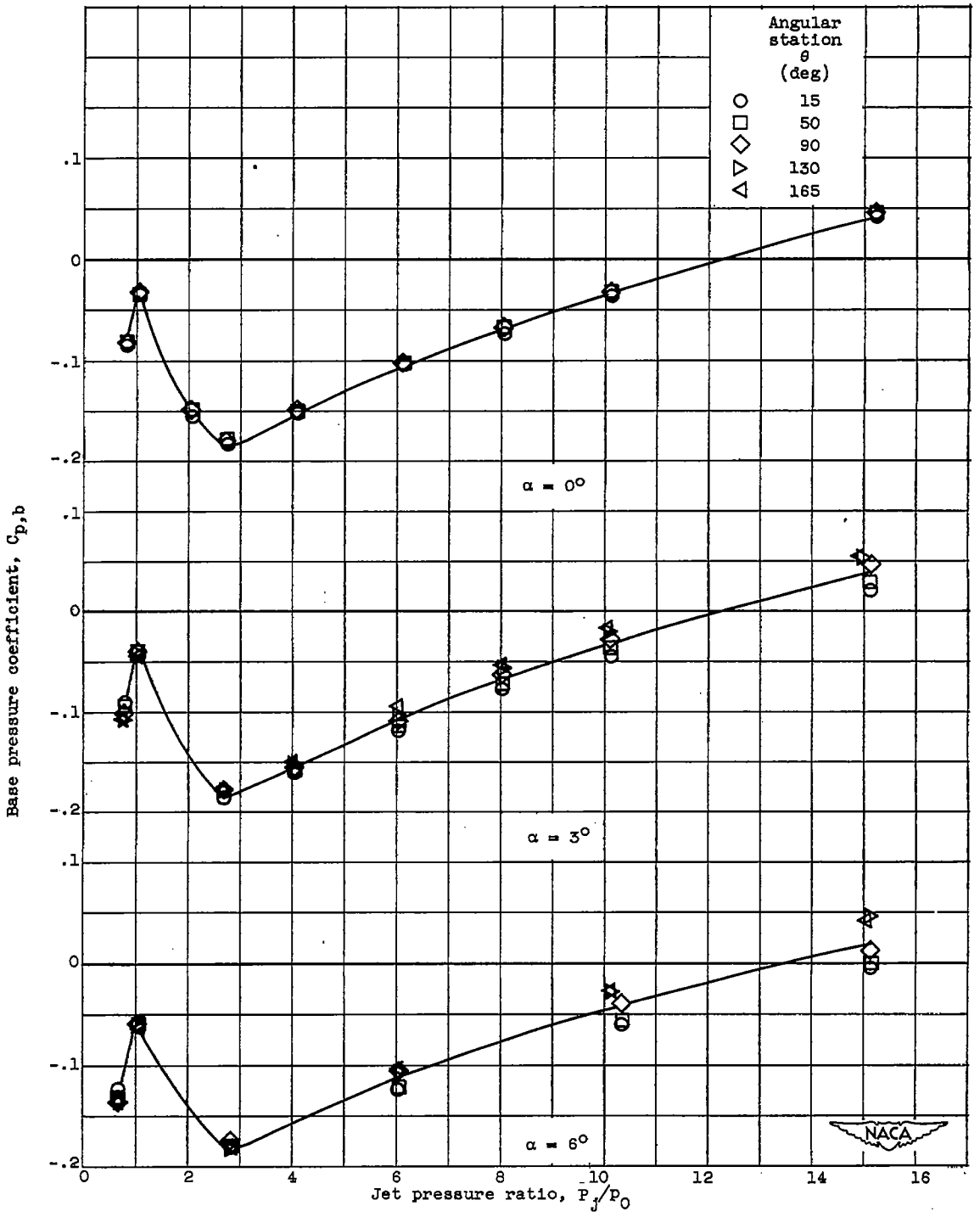

(b) $\epsilon = 5.63°$; $D_b/D_m = 0.704$.

Figure 26. - Continued. Variation of base pressure coefficient with jet pressure ratio for various angles of attack α, boattail angles ϵ, and base to body diameter ratios D_b/D_m.

8228

2228

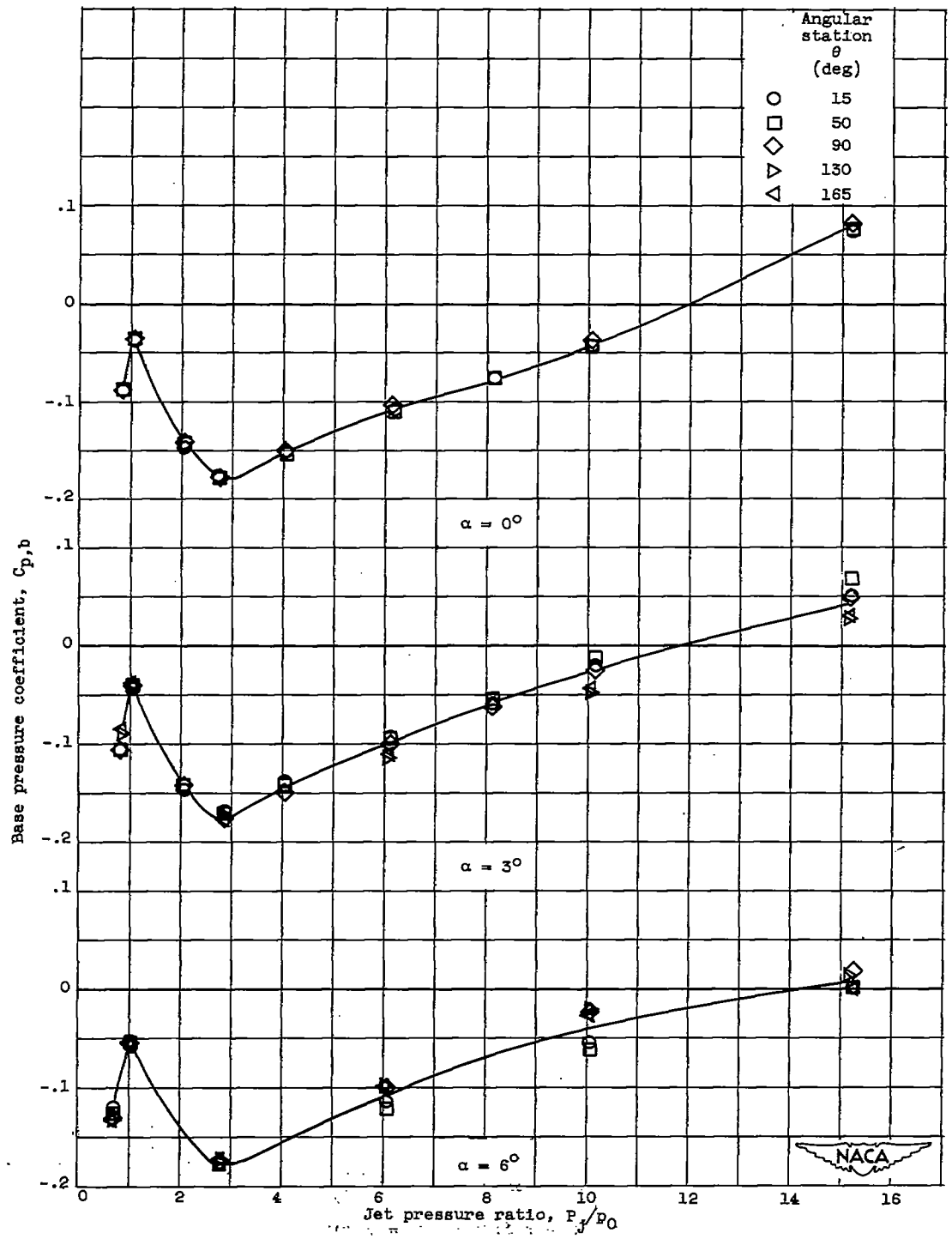

(c) ϵ = 7.03°; D_b/D_m = 0.704.

Figure 26. - Continued. Variation of base pressure coefficient with jet pressure ratio for various angles of attack α, boattail angles ϵ, and base to body diameter ratios D_b/D_m.

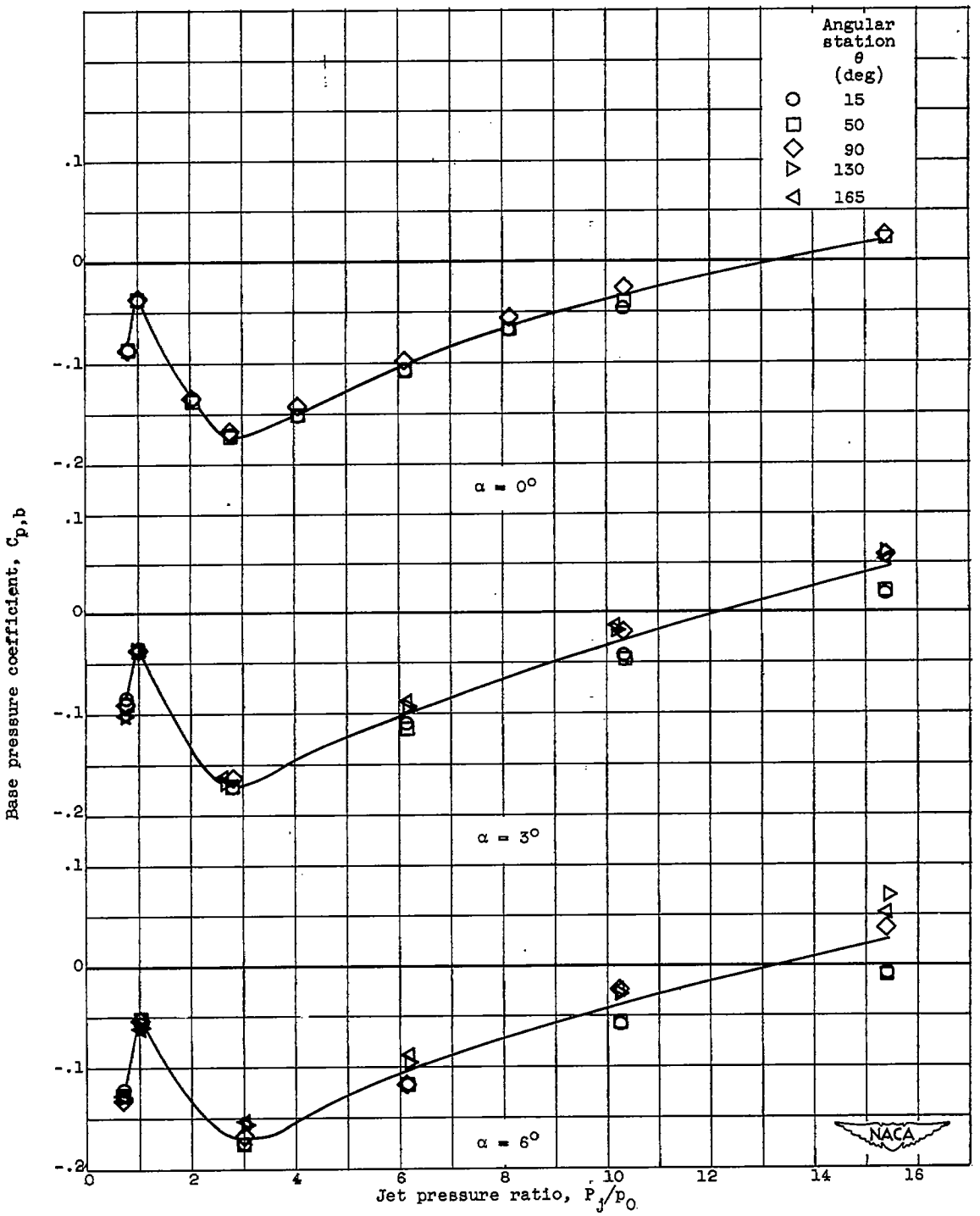

(d) ϵ = 9.33°; D_b/D_m = 0.704.

Figure 26. - Concluded. Variation of base pressure coefficient with jet pressure ratio for various angles of attack α, boattail angles ϵ, and base to body diameter ratios D_b/D_m.

2228

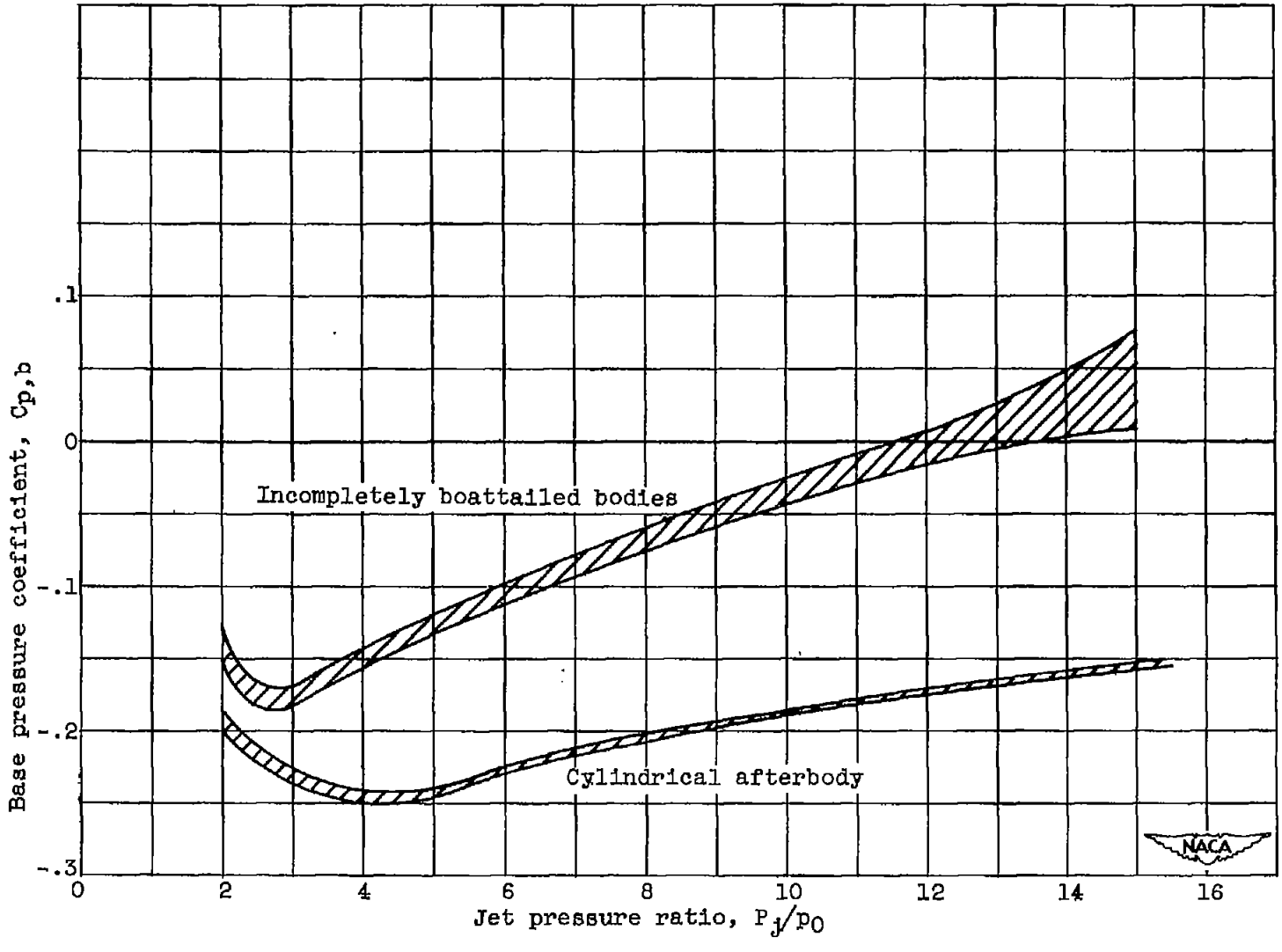

Figure 27. - Envelopes of mean variations of base pressure with jet pressure ratio for cylindrical afterbody and incompletely boattailed bodies at angles of attack from 0° to 6°.

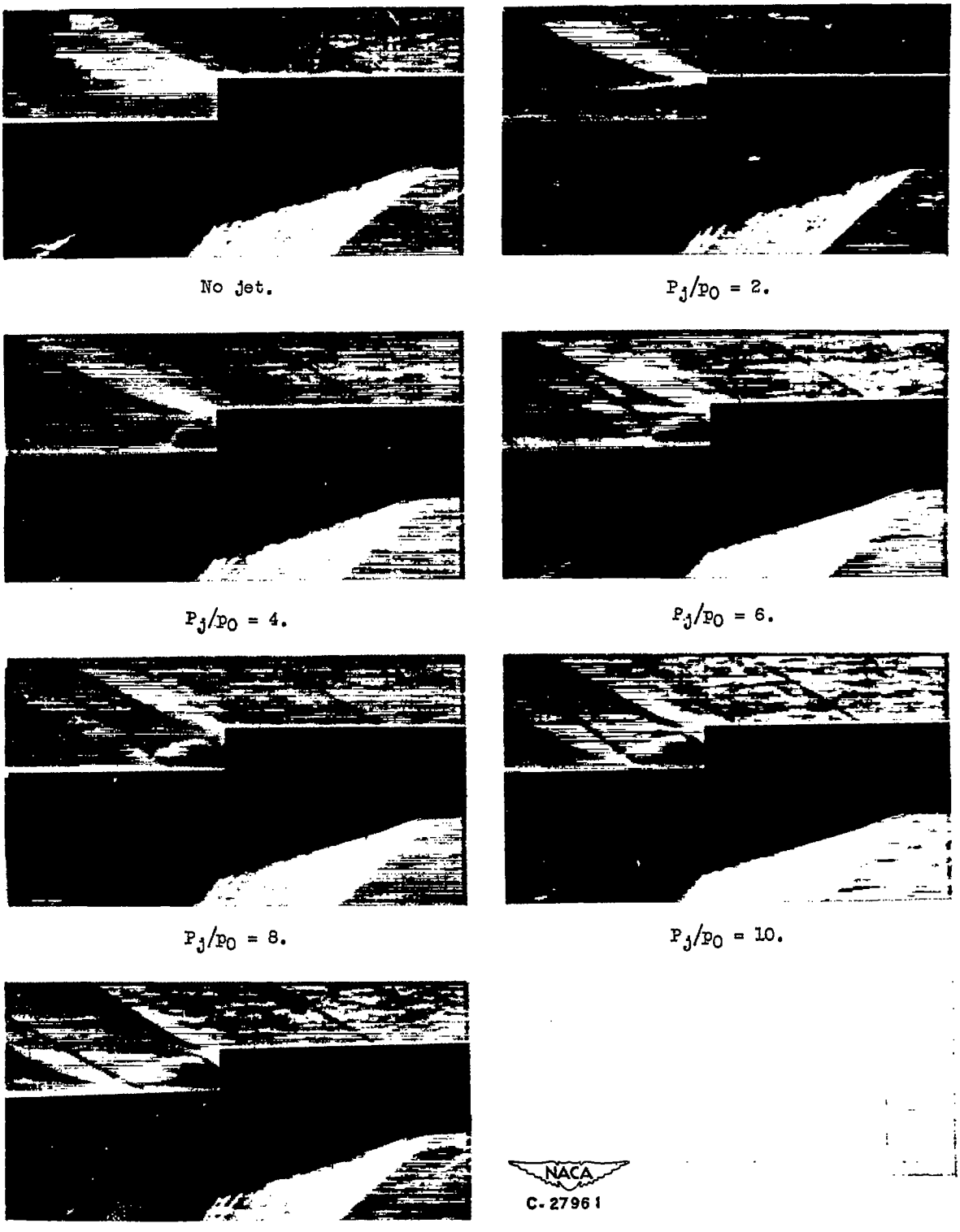

Figure 28. - Schlieren photographs of cylindrical afterbody for various jet pressure ratios P_j/p_0. Mach number M_0, 1.91; angle of attack α, 0°.

2228

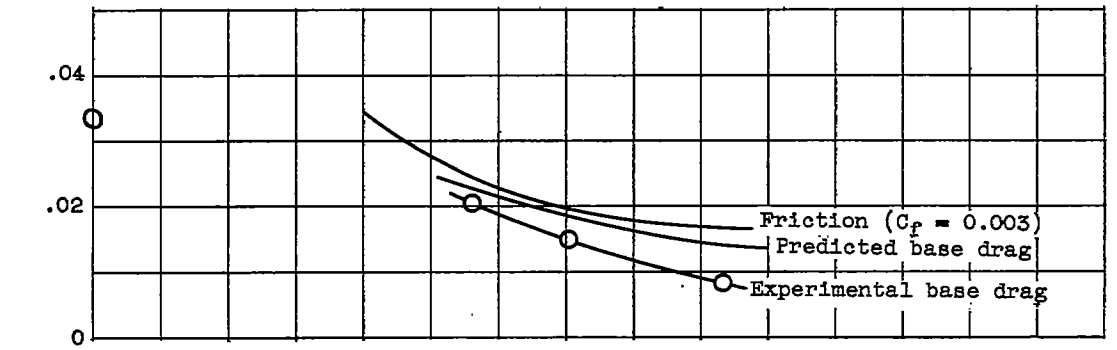

(a) Base pressure drag and friction drag.

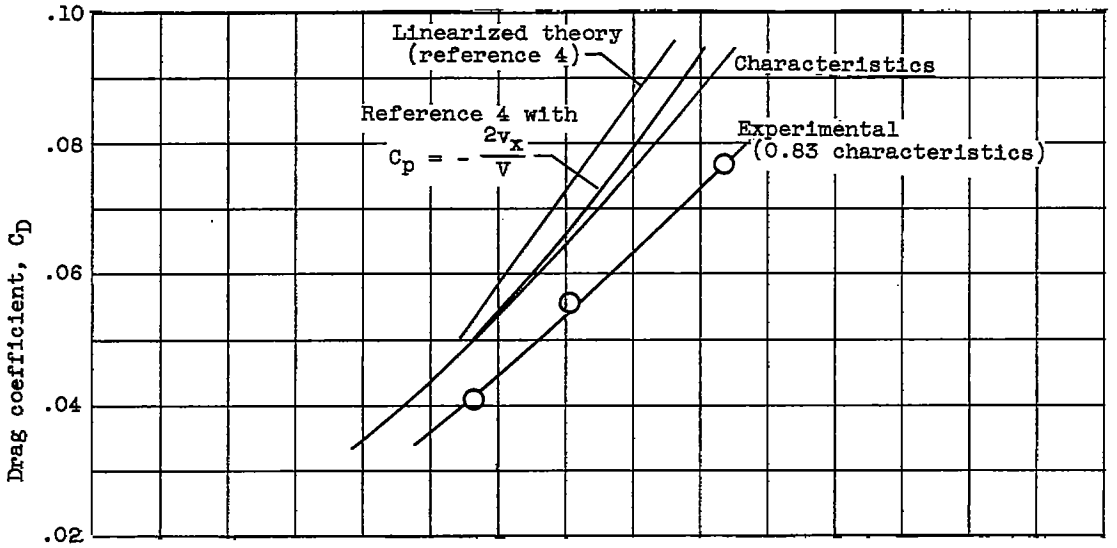

(b) Side pressure drag.

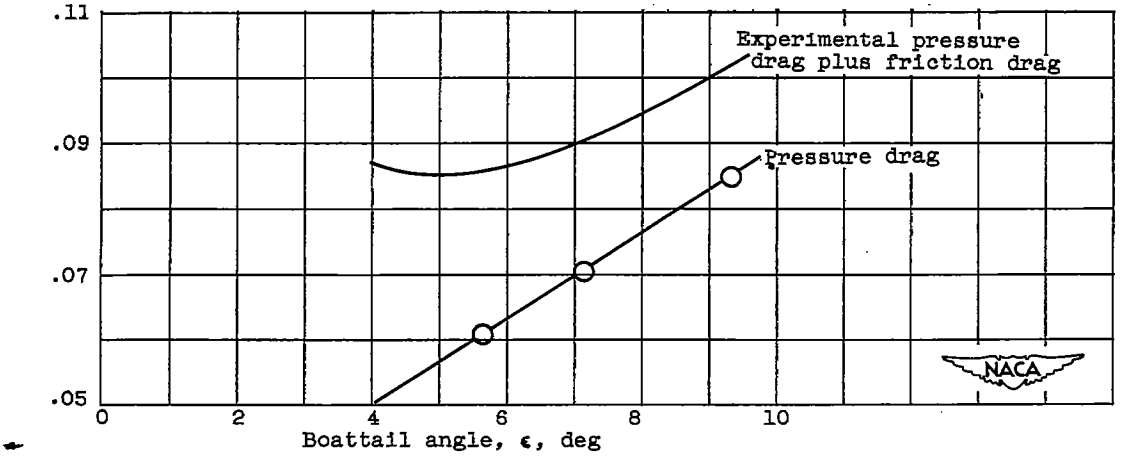

(c) Total drags.

Figure 29. - Variation of components of boattail drag coefficient with boattail angle. Angle of attack α, 0°, base to body diameter ratio D_b/D_m, 0.506; no jet flow.

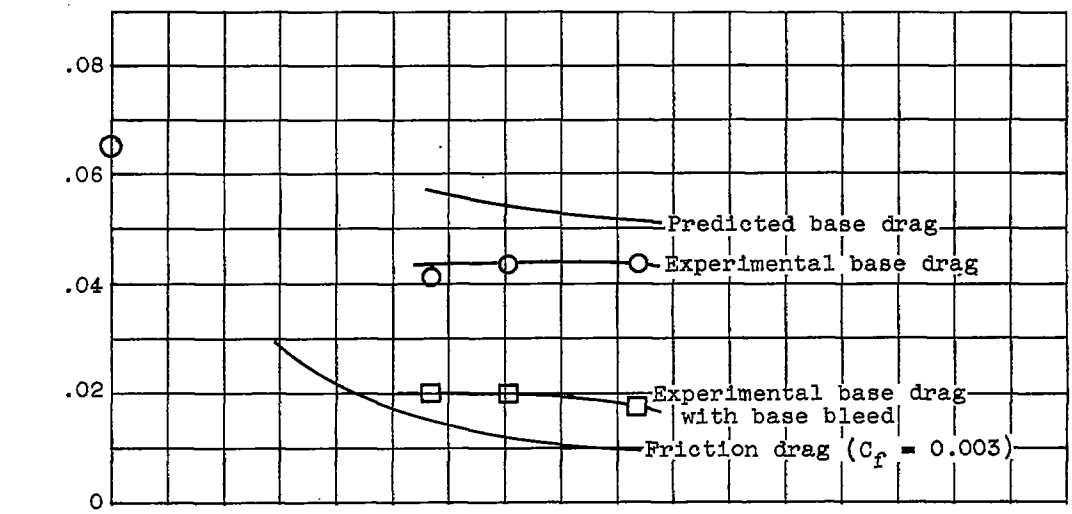

(a) Base pressure drag and friction drag.

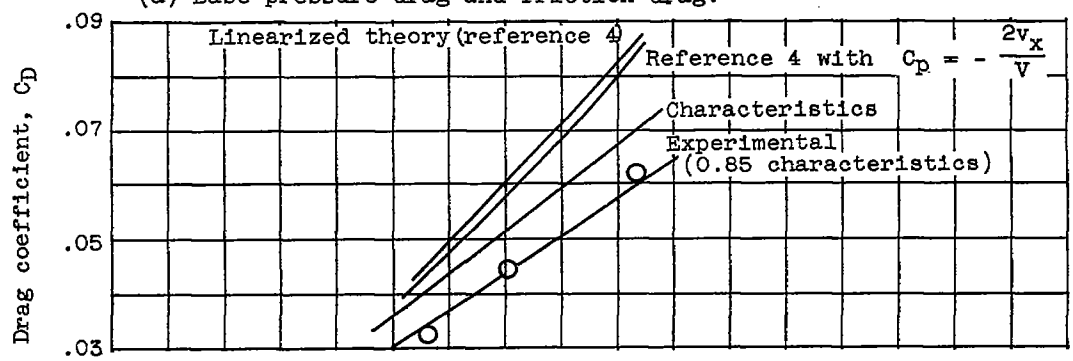

(b) Side pressure drag.

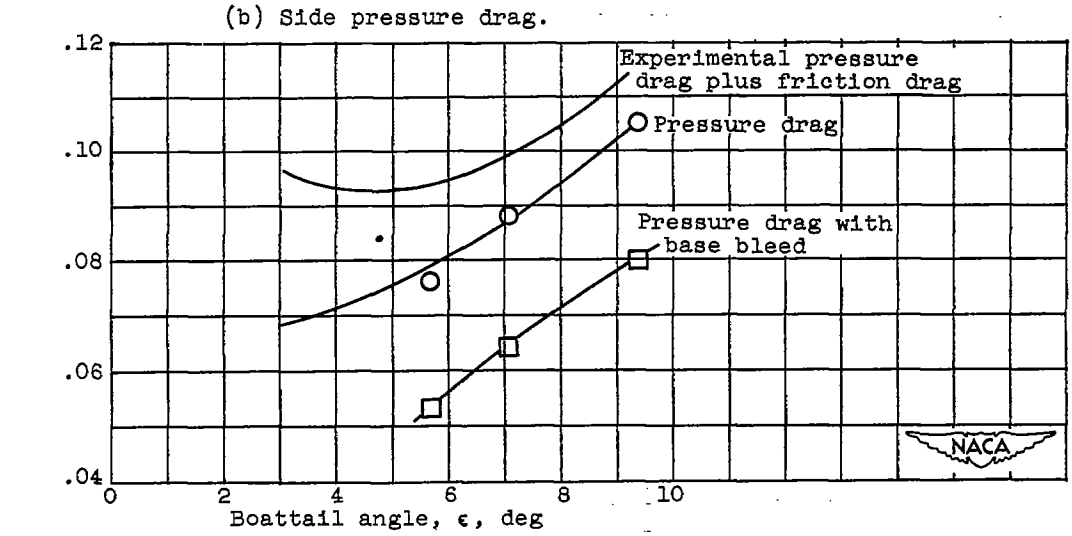

(c) Total drags.

Figure 30. - Variation of components of boattail drag coefficient with boattail angle. Angle of attack α, 0°; base to body diameter ratio D_b/D_m, 0.704; no jet flow.

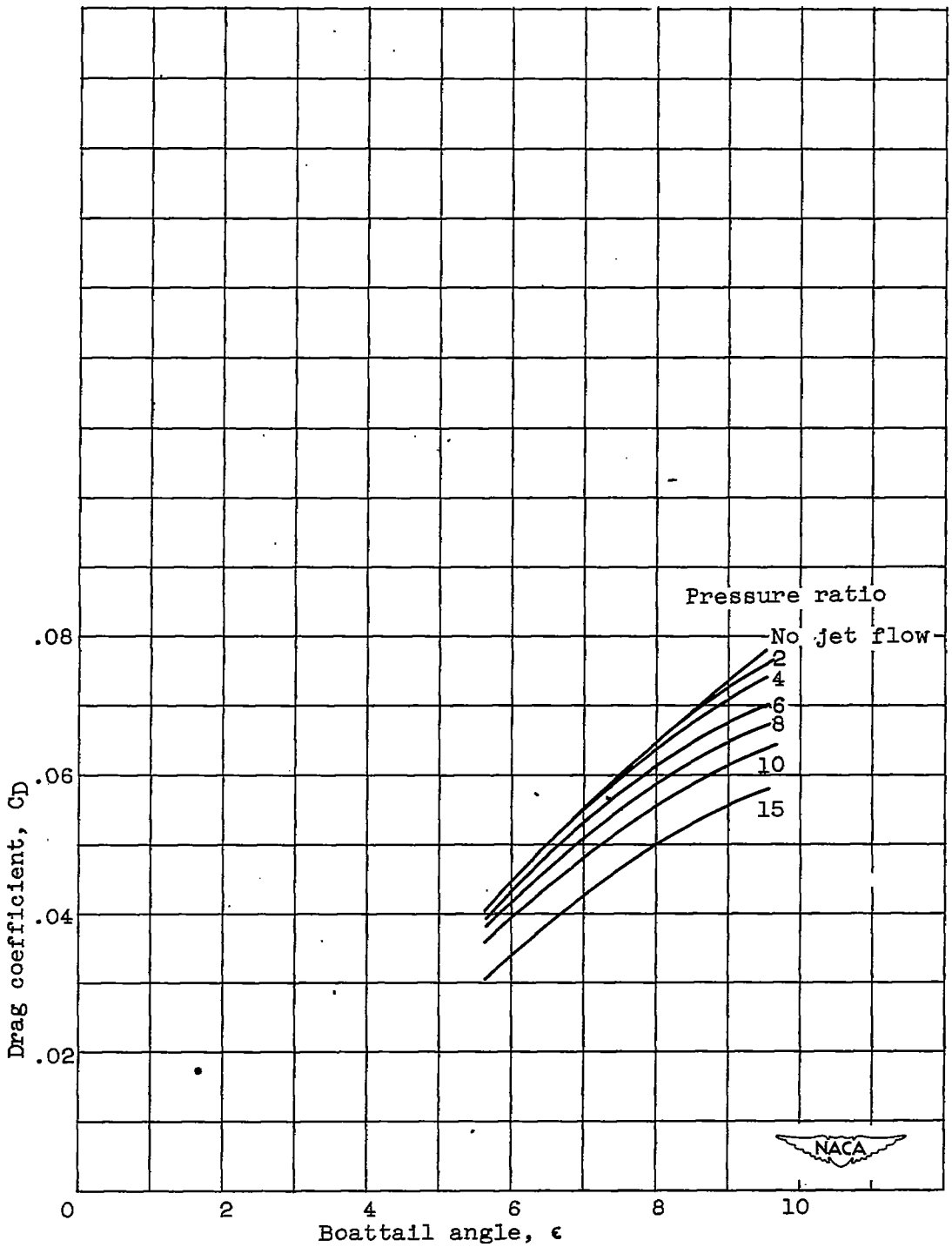

Figure 31. - Variation of boattail side pressure drag coefficient with boattail angle for various jet pressure ratios. Angle of attack α, 0°, base to body diameter ratio D_b/D_m, 0.506.

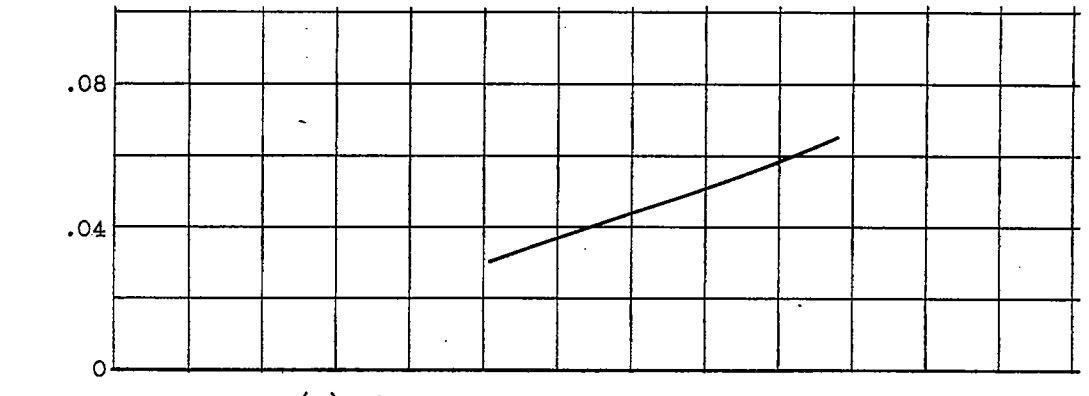

(a) Side pressure drag.

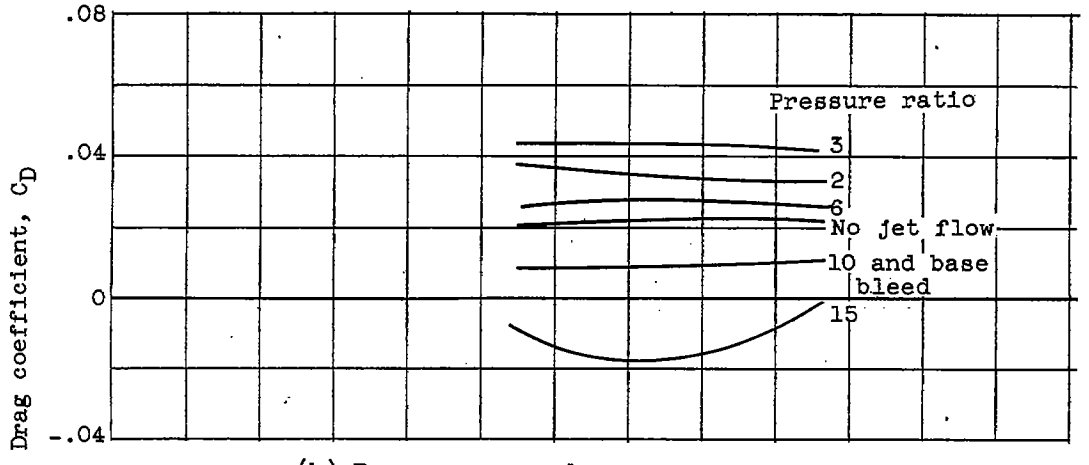

(b) Base pressure drag.

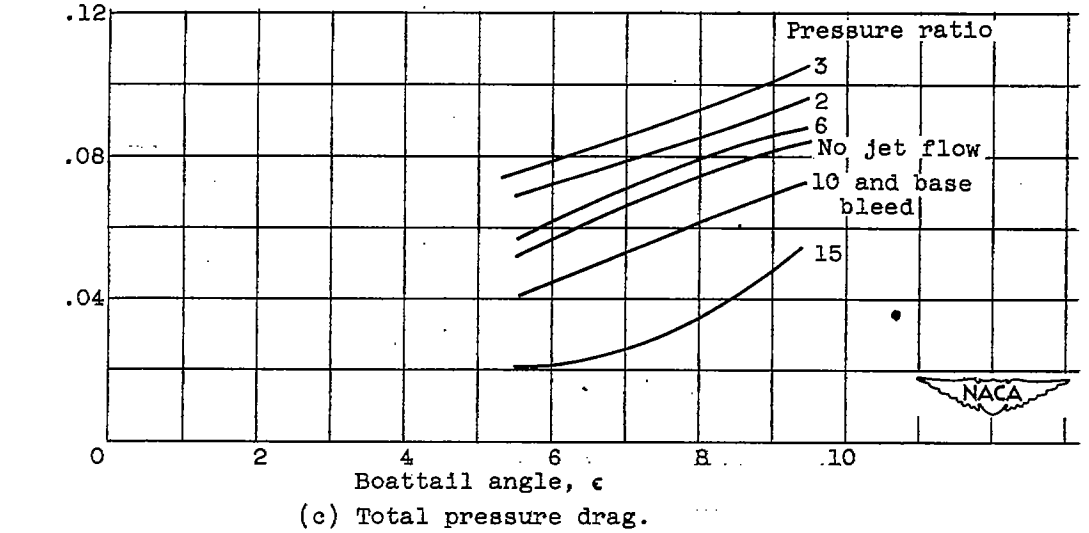

(c) Total pressure drag.

Figure 32. - Variation of side, base, and total pressure drag coefficient with boattail angle for various jet pressure ratios. Angle of attack α, 0°; base to body diameter ratio D_b/D_m, 0.704.

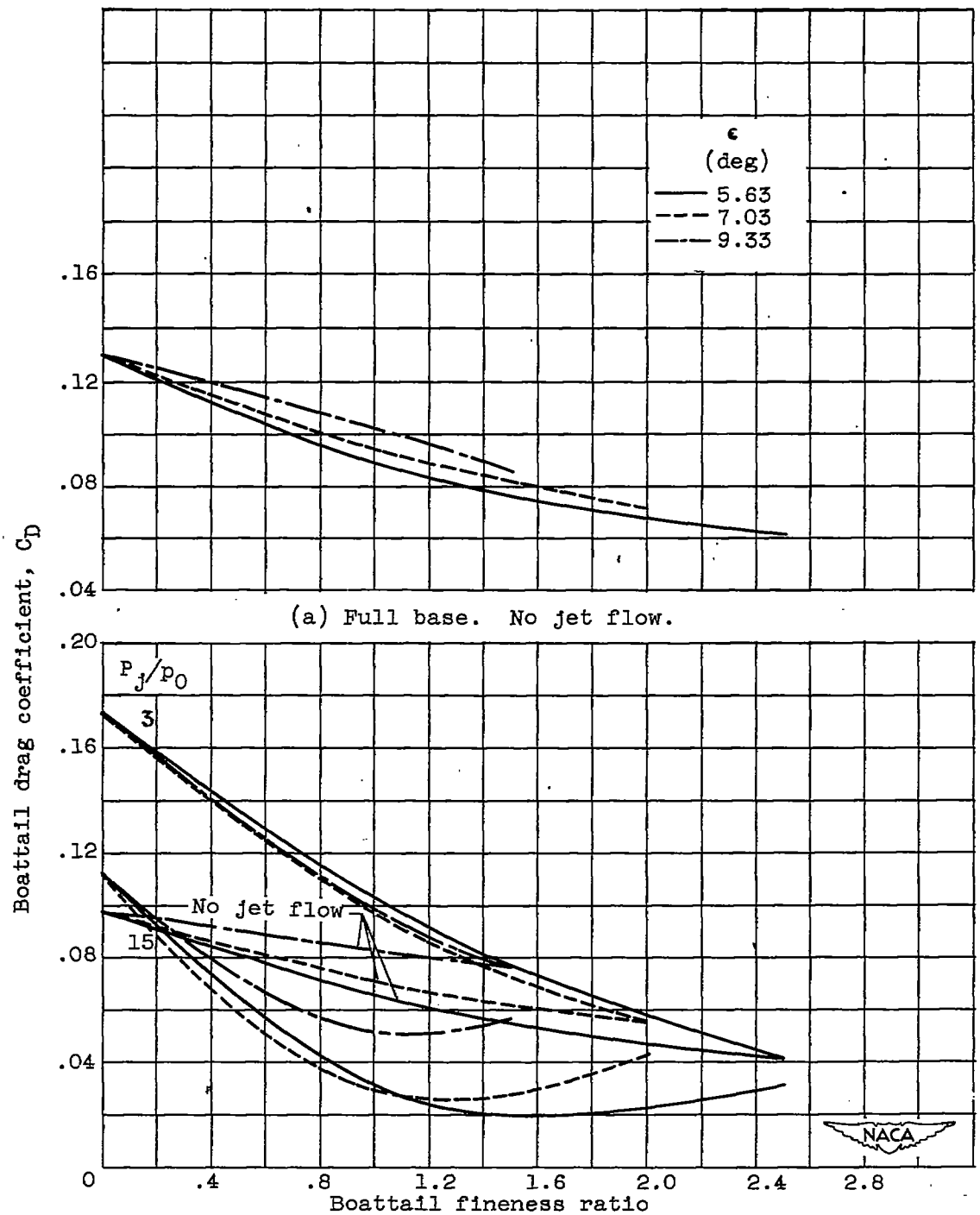

Figure 33. - Variation of boattail drag coefficient with boattail fineness ratio for various boattail angles ϵ and jet pressure ratios P_j/p_0.